



**Benha University
Benha Faculty of Engineering
Mechanical Engineering Department**

Investigation of Stabilized Flame for Lean Premixed and Pre-vaporized Biofuel Combustion

A thesis submitted in partial fulfillment of the requirements of the
M.Sc. in Mechanical Engineering

By

Belal Yehia Ibrahim El Saied Belal

B.Sc. of Engineering & Technology in Mechanical Engineering,
2014

Supervised by

Prof. Dr. Hany A. Moneib
Professor Emeritus of Combustion
Mechanical Power Engineering
Faculty of Engineering - Mattaria
Helwan University

Prof. Dr. Hesham M. El-Batsh
Professor of Energy Systems
Mechanical Engineering Department
Benha Faculty of Engineering
Benha University

Assoc. Prof. Ali M. A. Attia
Associate Professor
Mechanical Engineering Department
Benha Faculty of Engineering
Benha University

Benha 2018

The undersigned have examined the thesis entitled
**Investigation of Stabilized Flame for Lean
Premixed and Pre-vaporized Biofuel
Combustion**

Presented by

Eng. Belal Yehia Ibrahim El Saied Belal

B.Sc. of Engineering & Technology in Mechanical Engineering, 2014

a candidate for the degree of

M.Sc. in Mechanical Engineering

and hereby certify that it is worthy of acceptance

Prof. Dr. Mahmoud Abdul Rashid Naseer (Committee Chairperson)
Professor Emeritus of Combustion and Heat Engines,
Mechanical Power Engineering Department,
Faculty of Engineering – Ain shams University

Prof. Dr. Saad El-Din M. El-Said Habik (Committee Member)
Professor Emeritus of Combustion and Heat Engines,
Mechanical Power Engineering Department, Faculty of
Engineering of Port Said, Port Said University

Prof. Dr. Hany A. Moneib (Committee Member)
Professor Emeritus of Combustion and Heat Engines,
Mechanical Power Engineering Department,
Faculty of Engineering - Mattaria, Helwan University

Prof. Dr. Hesham M. El-Batsh (Committee Member)
Professor of Energy Systems
Mechanical Engineering Department,
Benha Faculty of Engineering, Benha University

Accepted from Mechanical Engineering Department

Assoc. Prof. Ahmed A. El-Betar (Department Chariman)

Accepted from the Postgraduate Affairs

Prof. Dr. Hesham M. El-Batsh (Vice Dean for Postgraduate Studies)

Accepted for the Faculty

Prof. Dr. Aref M. A. Soliman (Dean of the Faculty)

ABSTRACT

The considerable increase in energy demand, the strengthened requirements of new emission norms and the limited fuel resources are the major challenges for researchers over the world. The use of biodiesel produced from waste cooking oil is a promising solution. In the current study, the transesterification process used to convert waste cooking oil into a Waste Cooking Oil Methyl Ester (WCOME) has been modified and the production time is reduced with the help of ultrasonication. Then extensive study on combustor cold flow as well as flame characteristics had been carried out.

In the first set of experiments, the study compares the cold flow conditions (air), flame structure, combustion, and emission of Jet A-1 via the use of two swirl burners having different configurations and identical geometric swirl number ($SN=0.55$). The first configuration is a typical High Swirl Burner (HSB) with a central bluff body while the second one is a Low Swirl Burner (LSB) with central perforated plate allows relatively axial flow to pass through the burner center.

In the second set of experiments, the study identifies the effect of biodiesel blending ratio within mixtures of biodiesel/Jet A-1 fuel burned in a confined combustor on the flame characteristics and exhaust emissions. The Jet A-1 fuel is blended with WCOME with volume fraction of 5, 10, 15 and 20%, symbolized as B5, B10, B15, and B20 respectively. For all tested cases the Lean Pre-vaporized Premixed (LPP) turbulent flames are examined keeping the same equivalence ratio $\phi = 0.75$ and the temperature of premixed fuel/air mixtures entering the combustion chamber at 250 °C.

The main results indicated that the flow field of the LSB is free of a central recirculation zone while HSB has a large central recirculation region. The lean

pre-vaporized premixed Jet A-1 and air can sustain steady combustion at HSB and LSB with comparable global combustion quality. The HSB can generate an attached blue cone-shaped flame while the LSB can generate a blue lift-off “W” type flame. The HSB flame temperature distribution shows a high-temperature zone at the burner edge which represent a hot spot region while the LSB shows a more uniform flame temperature distribution. The CO and NO_x concentrations of the HSB through the flame are approximately 50 % higher than those for LSB. The local flame temperature distribution of the biodiesel/Jet A-1 fuel shows a similar behavior like that of Jet A-1. Biodiesel (oxygenated fuel) addition to Jet A-1 has a great effect on the emission characteristics of LPP combustion. There was remarkable emissions reduction due to biodiesel blending, the maximum reduction in CO was achieved for B20 as 30% lower than Jet A-1 and the maximum reduction for NO_x was achieved at B5 as 45% lower than Jet A-1. The Jet A-1 fuel can be replaced by biodiesel/Jet A-1 fuel without any modifications in the combustor design as they have similar temperature distribution and great emission reduction.

DEDICATION

To the one who is dearer than my soul
My first master, the master of all creatures

Prophet Mohamed (PBUH)

ACKNOWLEDGEMENT

First of all, I am so grateful to Allah for giving me the guidance, strength, patience, and hope to complete my research work successfully. It is the mercy of Allah and my trust in Him that have made such a dream to become a reality.

This work would not have been possible without the support and assistance of an uncountable number of people. To start, I would like to express my deep gratitude to my advisors Prof. Hany A. Moneib, Prof. Hesham M. El-Batsh, and Assoc. Prof. Ali M. A. Attia for their inspiring guidance, valuable advice, and constant encouragement throughout the progress of this research. Their suggestions, criticism, and patience have been a great asset. I have had a wonderful experience and have gained so much both personally and professionally.

I also want to appreciate all members of Benha Faculty of Engineering who are helpful, simple, and has good manners, and all of those who graciously gave me their time and assistance so that I could accomplish the requirements of this degree. Special thanks for Dr. Radwan El-zoheiry and Dr. Ahmed El-seesy who spent more time to support and help me during different stages of the work.

Last but not least, I would like to thank my family for their support and love during the past years of my college education. My friends are also worth thanking. I have benefited so much from having them around. Truly, I can't thank everyone enough.

CONTENTS

ABSTRACT	i
DEDICATION	iii
ACKNOWLEDGEMENT	iv
CONTENTS	v
List of Figures	viii
List of Tables	x
List of Abbreviations	xi
Nomenclature	xiii
1. Chapter 1: INTRODUCTION	1
1.1 Overview	1
1.1 Objectives of the Present Study	3
1.2 Thesis Layout	3
2. Chapter 2: LITERATURE REVIEW	5
2.1 Swirl Stabilized Combustors	5
2.1.1 Review on the geometry of low swirl burner	11
2.1.2 Review on low swirl burner emissions	12
2.2 Biodiesel	13
2.2.1 Transesterification reaction	14
2.2.2 The parameters affecting the transesterification reaction	15

2.3	Gas Turbine Emissions	17
2.3.1	Carbon monoxide (CO).....	18
2.3.2	Nitrogen oxides (NO _x)	18
2.4	Emissions Characteristics for Biodiesel in Gas Turbines.....	20
2.5	Research Aims	22
3.	Chapter 3: TEST FACILITY AND PROCEDURE.....	24
3.1	Biodiesel Production Procedures	24
3.2	Produced Biodiesel Evaluation.....	28
3.3	The Combustion Test Rig.....	32
3.3.1	Combustor and swirl burners	34
3.3.2	Air delivery system	36
3.3.3	Air heating system.....	37
3.3.4	Fuel supply system	38
3.4	Measuring Instruments	39
3.4.1	Cold flow measurements.....	39
3.4.2	Temperature measurements.....	42
3.4.3	Species concentrations measurement	42
3.5	Experimental Program and Procedures	43
3.6	Data Reduction and Analysis	45
4.	Chapter 4: RESULTS AND DISCUSSION.....	48
4.1	Experimental Program	48
4.2	Effect of Burner Configuration on the Cold Flow Pattern	49

4.3	Effect of Burner Configuration on the Combustion and Emissions Characteristics	56
4.4	Effect of Jet A-1/Biodiesel Blends on the Combustion and Emissions Characteristics of HSB.....	68
4.5	Effect of Jet A-1/Biodiesel Blends on the Combustor Thermal Uniformity.....	75
4.6	Environmental Impact of The Waste Cooking Oil Biodiesel.....	76
5.	Chapter 5: CONCLUSIONS	78
	REFERENCE	80
Appendix A	THERMOCOUPLES CALIBRATION	89
Appendix B	DATA ACQUISITION SYSTEM.....	90
Appendix C	CATALOGUES OF INSTRUMENTATIONS	95
	الملخص	102

List of Figures

Figure 2-1 Flow field of confined HSB, Chtereve et al. [15]	7
Figure 2-2 Flow field of LSB, Colorado[18]	9
Figure 2-3 Schematic representation of the aerodynamics of a confined (a) HSB, (b) LSB, Therkelsen [19].....	10
Figure 2-4 Stoichiometric transesterification reaction	14
Figure 3-1 Major steps to produce biodiesel using ultrasonic waves	25
Figure 3-2 Ultrasonic setup	26
Figure 3-3 Settling and separation process	27
Figure 3-4 Water washing process	27
Figure 3-5 Waste cooking oil biodiesel.....	28
Figure 3-6 Thermal analyzer setup.....	29
Figure 3-7 The thermogravimetric analysis of WCOME B100 and raw WCO	30
Figure 3-8 Elemental analyzer setup	31
Figure 3-9 Test rig schematic drawings	33
Figure 3-10 The LPP Combustor	34
Figure 3-11 The configurations of the present HSB and LSB	35
Figure 3-12 The main components of the air delivery system.....	37
Figure 3-13 The tip geometry of the five-hole probe and its coordinate system	39
Figure 3-14 Five-hole pressure probe and DAQ system.....	40
Figure 3-15 The flow chart for calculating the velocity components	41
Figure 3-16 Fine type R (platinum/platinum-13% rhodium) thermocouple. .	42
Figure 3-17 Gas analyzer	43
Figure 3-18 Sampling points.....	45
Figure 4-1 Measured axial velocity profiles	50

Figure 4-2 Contours of the normalized axial velocity; (a) HSB and (b) LSB	51
Figure 4-3 Measured radial velocity profiles	53
Figure 4-4 Contours of the normalized radial velocity; (a) HSB and (b) LSB	54
Figure 4-5 Contours of the total pressure (Pa); (a) HSB and (b) LSB	55
Figure 4-6 Measured radial temperature profile at combustor exit.....	57
Figure 4-7 Measured radial CO profile at combustor exit	57
Figure 4-8 Measured radial NO _x profile at combustor exit.....	57
Figure 4-9 Jet A-1 flame image; HSB (Left) and LSB (Right).....	58
Figure 4-10 Flame temperature radial distribution	60
Figure 4-11 Contours of the flame temperature; (a) HSB and (b) LSB	61
Figure 4-12 In flame CO concentrations radial distribution	63
Figure 4-13 Contours of the CO concentrations; (a) HSB and (b) LSB	64
Figure 4-14 In flame NO _x concentrations radial distribution.....	66
Figure 4-15 Contours of the NO _x concentrations; (a) HSB and (b) LSB.....	67
Figure 4-16 In flame temperature radial distribution	70
Figure 4-18 In flame CO concentrations radial distribution	72
Figure 4-19 In flame NO _x concentrations radial distribution.....	74
Figure 4-17 Combustor pattern factor for tested fuels	75
Figure 4-20 Emission index of nitrogen oxides	76
Figure 4-21 Emission index of carbon monoxide	77

List of Tables

Table 1-1 Feedstocks for biodiesel production.	2
Table 2-1 Review on the values of the swirler design variables	11
Table 2-2 Selected previous studies related to biodiesel emission in gas turbine applications	21
Table 3-1 Technical specifications of the used raw waste cooking oil	24
Table 3-2 Properties of the used fuels, Jet A-1 and waste cooking oil biodiesel	31
Table 3-3 Geometric dimensions of the present HSB and LSB.....	36
Table 3-4 Specifications of the devices used in the air heating system	38
Table 3-5 Resolution and range of gas analyzer for emission concentrations	42
Table 4-1 Test conditions of experiments	48

List of Abbreviations

Bx	Blend contains x% biodiesel and 100-x Jet A-1
CB	Center body
CDZ	Central divergent zone
CFM	Cubic foot per minute
CME	Canola methyl ester
CRZ	Central recirculation zone
DAQ	Data acquisition
D_{hub}	The swirler center body diameter
D_{sw}	The outer swirl annuals diameter
EA	Elemental analyzer
EI	Emission index
H_2SO_4	Sulfuric acid
HCl	Hydrochloric acid
HSB	High swirl burner
IRZ	Inner recirculation zone
ISL	Inner shear layer
JAME	Jatropha methyl ester
JAPO	Jatropha pure oil
JME	Jojoba methyl ester
KOH	Potassium hydroxide
LPP	Lean pre-vaporized premixed
LSB	Low swirl burner
NaOH	Sodium hydroxide
ORZ	Outer recirculation zone
OSL	Outer shear layer

PF	Pattern factor
PIV	Particle image velocimetry
PME	Palm methyl ester
Pt	Platinum
Rh	Rhodium
RME	Rapeseed methyl ester
SME	Soybean methyl ester
SN	Swirl number
TCD	Thermal conductivity detector
TGA	Thermogravimetric analysis
UHC	Unburned hydrocarbon
WCO	Waste cooking oil
WCOME	Waste cooking oil methyl ester

Nomenclature

List of Symbols

$ V $	Velocity magnitude	[m/s]
A	Area	[m ²]
C_p	Specific heat at constant pressure	[J/kg.K]
D	Diameter	[m]
h	Local heat transfer coefficient	[W/m ² K]
HHV	Higher heating value	[MJ/kg]
K	Thermal conductivity of air	[W/m.K]
L	Length	[m]
LHV	Lower heating value	[MJ/kg]
\dot{m}	Mass flow rate	[kg/hr]
M_w	Molecular weight	[kg/kmol]
Nu	Nusselt number	[-]
Pr	Prandtl number	[-]
Q	Volume flow rate	[m ³ /hr]
R	Gas constant	[J/kg.K]
R	Burner radius	[m]
r/R	Relative distance from burner center	[-]
Re	Reynolds number	[-]
Ru	Universal gas constant (8314)	[J/kmol.K]
T	Temperature	[K]
Z	Vertical distance from the burner tip	[m]
P	Static pressure	[Pa]
P_t	Total pressure	[Pa]

k_s	The static pressure coefficient	[-]
k_t	Total pressure coefficient	[-]
k_α	Pitch angle coefficient	[-]
k_β	Yaw angle coefficient	[-]
\bar{p}	Mean pressure	[Pa]
u	Velocity – x direction	[m/s]
v	Velocity – y direction	[m/s]
w	Velocity – z direction	[m/s]

Greek Symbols

μ	Dynamic viscosity	[kg/m.s]
ε	Emissivity	[-]
$\phi = \frac{\text{actual}_{\text{air}}^{\text{fuel}} \text{ratio}}{\text{theoretical}_{\text{air}}^{\text{fuel}} \text{ratio}}$	Equivalence ratio	[-]
ρ	Fluid density	[kg/m ³]
α	Pitch angle of 5-hole probe	[°]
σ	Stefan Boltzmann constant	[W/m ² K ⁴]
θ	Vane angle of swirler	[°]
β	Yaw angle of 5-hole probe	[°]

Chapter 1: INTRODUCTION

1.1 Overview

The intensive consumption of fossil fuels in all sectors such as power generation, industrial processes, and transportation has engendered extensive research to find new alternative fuels. Fossil fuels are non-renewable sources of energy which generate environmental pollutants that are related to global warming, climate change, and even some incurable diseases. The use of biofuels and their mixtures with fossil fuels to provide energy demands is one of the notable options. Unlike fossil fuels, which are finite, the biofuels are renewable, environmentally friendly and economically competitive. Biodiesel is the general name for the like-diesel compounds which can be produced from edible and non-edible vegetable-based oils, animal's fats and even waste cooking oil. Biodiesel has gained considerable attention since it is renewable, biodegradable, non-toxic, higher cetane number, higher flash point, lower emission of carbon monoxide, particulate matters, unburnt hydrocarbon, sulfur and volatile organic compounds as compared to conventional diesel [1].

The feedstocks used for biodiesel production can be categorized into three generations as shown in Table 1-1. The edible oils like soybean, rapeseed, palm, castor etc. are categorized as first-generation feedstocks of biodiesel. Of course, the first-generation feedstocks are available but their use as biofuel feedstock is of great concern because they contend with food materials. So, researchers started to use oils derived from non-edible crops like Jatropha and Jojoba categorized as second-generation feedstocks of biodiesel. The main advantage of using second-generation feedstocks is that there will be no food issue and they can be grown in non-agricultural land in the desert and irrigated by waste water. The problem of the second generation is that a few farmers are

cultivating the second-generation crops. The third-generation feedstocks overcome the difficulties faced by previous generation feedstocks such as affecting food chain, economic feasibility, and availability [2].

Table 1-1 Feedstocks for biodiesel production.

Edible oil (1st generation)	Non-edible oil (2nd generation)	Other sources (3rd generation)
Rapeseed oil [3]	Jatropha curcus [6]	Waste cooking oil [8]
Palm oil [4]	Jojoba [7]	Chicken fat oil [9]
Castor oil [5]		Fish oil [10]
Soybean oil [6]		Micro algae [10]

Neat biodiesel and its blends with fossil fuels in various proportions reduced the unwanted toxic emissions like Unburned Hydrocarbons (UHC), Carbon Monoxide (CO) and smoke level where as it augmented the emissions like Carbon Dioxide (CO₂) and Nitrogen Oxides (NO_x) [2]. Further reduction in pollutant emissions can be also attained with the help of combustion improving techniques. One of these techniques is the lean pre-vaporized premixed (LPP) combustion. In this concept, the liquid fuels are burned via premixed combustion rather than diffusion combustion and so the corresponding complexities in diffusion flames are removed. At the case of lean combustion, the flame temperatures become lower leading to reducing the formation of thermal NO_x. Unfortunately, lean combustion operates near the lean flammability limit, where the flame approaches the conditions of its instability. Flame stabilization is usually accomplished by using a swirl burner. In order to operate gas turbine engines with biodiesel, the flame structure and the

combustion characteristics inside gas turbine combustion chambers must first be well understood.

1.1 Objectives of the Present Study

The present study aims to provide a detailed experimental comparison of the cold flow, the combustion and the emissions characteristics for two swirl burners having the same swirl number but having different designs configurations using LPP combustion technique. The study also aims to produce biodiesel from waste cooking oil to get waste cooking oil methyl ester (WCOME) following the transesterification process using ultrasonic and experimentally study the combustion characteristics of different Jet A-1/WCOME blends on the combustion and the emissions characteristics of LPP flame. These objectives can be realized by performing the following tasks:

- 1- Collecting waste cooking oil as feedstock for biodiesel production
- 2- Make the necessary filtration and cleaning of the collected waste oils
- 3- Produce the biodiesel from waste cooking oil under optimal conditions to get the highest yield and the acceptable biofuel viscosity.
- 4- Design low swirl and high swirl burners having the same swirl number.
- 5- Carry out extensive studies on the combustor cold flow as well as flame characteristics.

1.2 Thesis Layout

The thesis comprises five chapters, including the present one as an introduction. In **Chapter 2**, a detailed review of previous investigations related to gas turbine swirl stabilized combustors, gas turbine emissions, and the effect of biodiesel on the gas turbine emissions. This chapter is concluded with a detailed aim of the present investigation. **Chapter 3** describes the experimental

apparatus and the measuring techniques used. Error analysis, as well as the required analysis of the measured values, are presented in this chapter. **Chapter 4** is devoted to the description of the experimental program, presentation, and discussion of the experimental results. **Chapter 5** presents a summary and conclusions of the present investigation together with recommendations for future studies.

Chapter 2: LITERATURE REVIEW

A detailed study was performed to review the past research as well as to extend knowledge in the area of lean pre-vaporized premixed swirl stabilized biodiesel combustion. In this chapter, the past work related to gas turbine swirl stabilized combustors are reviewed. Then the motivations of biodiesel, biodiesel production, gas turbine emissions and the effect of biodiesel on gas turbine emissions will be discussed. After that, a review about lean pre-vaporized premixed combustion will be introduced. Finally, the research aims will be formulated.

2.1 Swirl Stabilized Combustors

The gas turbine is an internal combustion engine that is used for power generation and aircraft propulsion. A lot of researches and developments have been done to satisfy a wide range of combustor design and its functional requirements including high combustion efficiency, wide range of flame stability, low pressure loss, low emissions and pollutant species, durability, maintainability, and avoidance of combustion instabilities [11]. Two major combustion modes are used in gas turbines combustors, diffusion mode, and premixed mode. In the diffusion combustion mode, fuel and air entered the combustor in separate streams (without mixing) and the combustion occurred near stoichiometric air to fuel ratios at high temperatures. Any improper mixing between incoming reactants leads to the incomplete combustion. Moreover, as combustion temperature is close to the adiabatic flame temperature, there is a great tendency for the formation of thermal NO_x . The incomplete combustion, as well as the NO_x emissions, can be reduced if the premixed combustion mode is used where air and fuel are mixed upstream of

the combustor. The use of lean fuel conditions leads to combustion at lower temperatures and so lower thermal NO_x formation. However, the use of a very lean mixture near the lean blow-off limit can lead to unstable combustion. Maintaining flame stability is an important requirement for gas turbine combustors. A flame is locally stabilized when the flame speed equals the local mean velocity, which means that the flame is stationary at the desired location and is resistant to blowoff, flashback, and liftoff [12]. Swirl stabilization is the predominant mechanism to control flame stability as well as combustion intensity. Swirl can be produced geometrically by vane swirler, mechanically by rotation or aerodynamically by tangential injection into a flow stream [13]. Swirl flow can be characterized by the swirl number (SN), representing the ratio of the axial flux of angular momentum to the axial flux of axial momentum [14]. For swirl number higher than 0.6, the swirl is strong enough to create a toroidal reversal flow along the axis of the flow [11]. The reverse flow entrains and recirculates a portion of the hot combustion products to mix with the incoming reactants to stabilize the flame [11]. The recirculation zone provides good mixing and strong shear region, high turbulence, rapid mixing rates and long residence time [14]. The flow recirculation is generated by the low static pressure in the central core of the combustor downstream of the swirler. The swirl burners where recirculation zones are clearly formed are called high swirl burners (HSB) characterized by high swirl flow and the existing of center cylindrical solid body and the corresponding swirl number can be expressed as [14]:

$$SN = \frac{2}{3} \left[\frac{1 - \left(\frac{D_{hub}}{D_{SW}}\right)^3}{1 - \left(\frac{D_{hub}}{D_{SW}}\right)^2} \right] \tan \theta \quad \text{Equation 2-1}$$

Where, D_{hub} is center body radius, D_{SW} is the swirler radius and θ is the swirl vane angle. High swirl burner can operate with both non-premixed and premixed combustion. In the non-premixed combustion, the recirculation zone is the primary mechanism for enhancing the mixing of the fuel and air. For the premixed combustion, the recirculation zone entrains the incomplete combustion products to the primary reaction zone and mixes them with the fresh reactants. The flow field of a confined high swirl burner consists of six main fluid mechanic features which are identified by Chtereve et al. [15] as shown in Figure 2-1. (A) outer recirculation zone (ORZ), (B) inner recirculation zone (IRZ), (C) A high velocity swirling jet that divides these recirculation zones, (D) the inner shear layer (ISL) that separates the swirling jet and the inner recirculation zone, (E) the outer shear layer (OSL) that separates the swirling jet and the outer recirculation zone. (F) The center body wake.

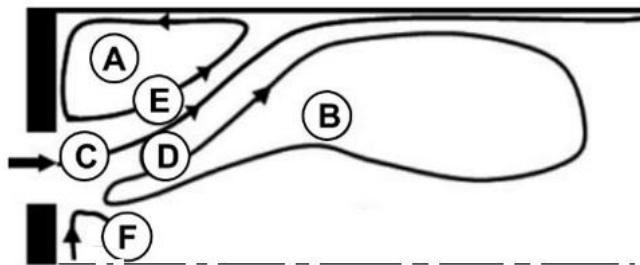


Figure 2-1 Flow field of confined HSB, Chtereve et al. [15]

A promising alternative for the high swirl combustion is low swirl combustion where the swirl number is lower than 0.6. The low swirl burners (LSB) are the designed configuration to produce weak swirl flow where the low axial pressure gradient is not strong enough to cause recirculation of the flow. The essential flame stabilization mechanism of LSB is divergent flow rather than

recirculation zones. The LSB consists of two concentric cylinders, the outer annulus provides swirl to the flow, and the central jet allows relatively undisturbed flow to pass through. A perforated sheet serves as the blockage in the center of the burner that controls the flow split between the inner (unswirled) and outer (swirled) region. Generally, the SN of LSB can be determined depending on three main geometrical parameters; including the ratio of the center channel radius to the burner radius ($R = R_c/R_b$), the vanes' angle (θ), and the ratio of the mass flux of the unswirled flow to the mass flux of swirled flow (known as mass flow split $m = m_c/m_s$) [16] using the following relation [17]:

$$SN = \frac{2}{3} \tan \theta \frac{1-R^3}{1-R^2+m^2((1/R^2)-1)^2 R^2} \quad \text{Equation 2-2}$$

A schematic representation of the LSB flow fields is shown in Figure 2-2. The flow field is divided into an outer swirling region and a non-swirling inner region. A portion of the flow enters the central channel and flow in the axial direction (x-direction), the remaining flow crossing the outer swirling annulus of the burner which directed it in tangential and radial direction. This creates a divergent flow that generates a decaying velocity profile along the centerline.

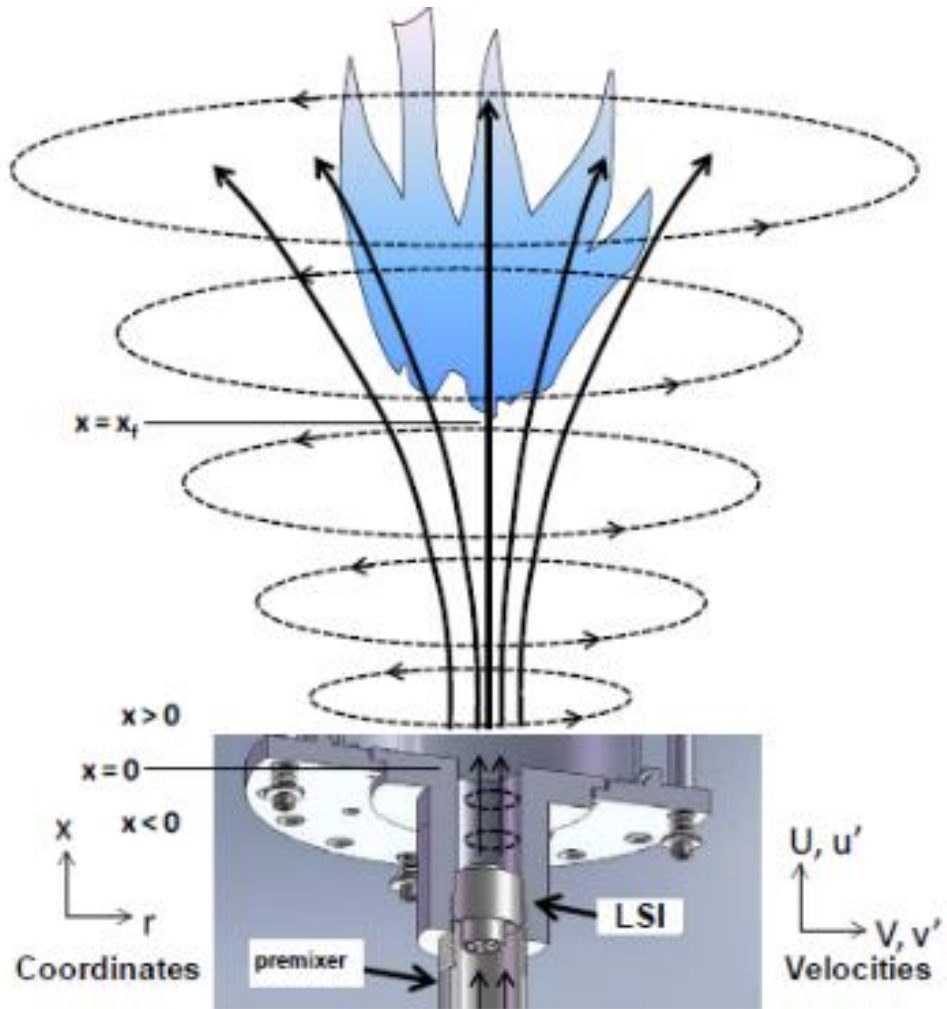


Figure 2-2 Flow field of LSB, Colorado[18]

Figure 2-3 provides schematics representation of a comparison between the aerodynamics of a confined HSB and LSB [19]. As mentioned before, the HSB has a central recirculation zone (CRZ) while the LSB has a central divergent zone (CDZ).

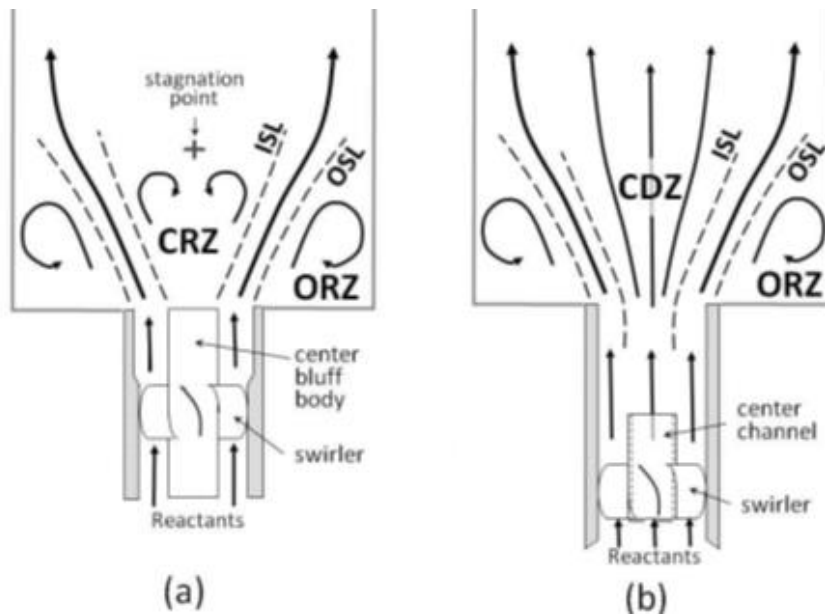


Figure 2-3 Schematic representation of the aerodynamics of a confined (a) HSB, (b) LSB, Therkelsen [19].

Johnson et al. [20] carried out a comparison between high swirl burner (HSB) ($SN=0.73$) and the same burner modified for operation as a low swirl burner (LSB) ($SN=0.5$). The measurements of the flow fields were performed at atmospheric conditions and also at gas turbine relevant conditions of elevated temperature and pressure using PIV. The measurements of the flow fields for both burners demonstrated that the LSB is free of recirculation while the HSB has large recirculation zones. Littlejohn et al. [21] conducted laboratory experiments to investigate the fuel effects on the turbulent premixed flames produced by a gas turbine LSB. The analysis of the normalized velocity statistics showed that the non-reacting and reacting flow fields of the LSB have similar features. Legrand et al. [22] performed stereoscopic PIV measurements for both a conventional HSB and LSB. The results indicated that the LSB has a reduced recirculation zone in comparison with the HSB configuration. The

authors concluded that the flame in the LSB is stabilized by means of a low velocity zone more than by the recirculation zone. Authors also noted that asymmetries were presented in the mean flow fields of low swirl flames due to the rotation of low-velocity structures about the inner core axial flow. It can be concluded that the use of HSB would be more effective for diffusion flames rather than for premixed flames to get better mixing but there will be a zone of intense shear and so expected higher local temperature.

2.1.1 Review on the geometry of low swirl burner

The following section presents some of the design constraints of LSB used in the previous studies as well as a brief description of its configurations.

Therkelsen, et al.[16], performed a parametric study on different geometrical configuration of LSB for methane burned in the open atmosphere to conclude the constraint for LSB design. The results demonstrated that SN should be between 0.4 and 0.55. The swirler can have straight or curved vanes with angle α from 37° to 45° . The optimum center channel to burner radius ratios R can be from 0.5 to 0.8. In addition, the exit length L can be from 2 to 3 times the burner radius R_b . Data summarized in Table 2-1 collects the design parameters of LSB used in previous studies cited in the literature.

Table 2-1 Review on the values of the swirler design variables

Ref	Number of vanes	Vane angle α	$R = \frac{D_{hub}}{D_{sw}}$	Blockage ratio	Swirl number
Therkelsen et al. [16]	16	32, 37 and 42	0.52, 0.67 and 0.8	-	From 0.4 to 0.55
Cheng et al. [23]	16	40	0.63	58%	0.51

Ref	Number of vanes	Vane angle α	$R = \frac{D_{hub}}{D_{sw}}$	Blockage ratio	Swirl number
Littlejohn et al. [24]	8	37	0.776	71%	0.4
Cheng et al. [25]	16	40	0.66	-	0.5
Johnson et al. [20]	16	45	0.63	58%	0.5
Day et al. [26]	8	37	0.76	78%	0.55

Feyz et al [27] investigated the effect of burner exit length on the combustion characteristics of LSB operating on natural gas. The results showed that, the increase in the exit length from $1 D_{sw}$ to $1.5 D_{sw}$ significantly improves the temperature uniformity, increases the flame heat exchange to the walls relatively by 4.9% and limits the stack losses at 28%.

Cheng et al [23] studied the effects of combustor geometry on the flame and flow field properties of a LSB configured for burning of hydrocarbon and hydrogen fuels in gas turbines by changing the diameter of the confined tube attached at the exit plane of the burner. The PIV measurements result reported that the supply of un-swirled flow through the center channel of LSB retards the formation of a central recirculation zone occurred at combustor exit and promotes the formation of flow divergence occurred above burner rim. The optimum expansion ratio needed to decrease the recirculation zones occurred when the enclosure radius is about three times larger than the burner radius i.e. 3:1.

2.1.2 Review on low swirl burner emissions

From the literature, it can be noticed limited works cited where the emissions using LSB are investigated. Among the available literature, Johnson et al. [20] carried out a comparison between emissions formed using HSB (SN=0.73) and

that of using LSB (SN=0.5). The measurements demonstrated that the NO_x emissions of LSB were 60% lower than those of HSB, but the CO emissions were comparable under the same operating range. Koyama et al. [28] investigated the adaptation of the liquid-fueled LSB for industrial gas turbine combustor application over a wide range of inlet conditions and equivalence ratios. The results revealed that the NO_x emissions were reduced and met the Japanese regulation limits for liquid-fueled burners. Sequera et al [29] reported emissions measurements for a LSB operated by combustible gaseous mixtures of methane (CH₄), hydrogen (H₂), and carbon monoxide (CO) to simulate synthetic gas produced by coal gasification. The experiments were conducted at atmospheric pressure and the reactants were at room temperature (T=293K). Results showed, that the NO_x emissions for simulated syngas fuel mixtures are correlated with the adiabatic flame temperature. The CO emissions increased with the increase in the adiabatic flame temperature. Measured NO_x and CO emissions profiles show that the structure of turbulent flames from the LSB are similar to those for laminar premixed flames. From these limited works, it can be concluded that the use of LSB has a great effect on emission reduction globally better than that of HSB.

2.2 Biodiesel

The limitation of fossil fuel resources such as coal, petroleum oil, natural gas, etc. and the increase of environmental pollution force the scientific community to find alternative fuels with low emissions to be used in different combustion devices. One of the promising alternatives that can substitute petroleum diesel fuels is the biodiesel. Biodiesel is the general name for the like-diesel biofuel produced from edible and non-edible vegetable-based oils, animal's fats and even waste cooking oil.

Waste cooking oils biodiesel offer great potential beside its closed-loop energy cycle due to its substantial economic and environmental benefits. One of the most advantageous of burning waste cooking oil biodiesel is that it releases purely biogenic carbon, as it is derived from plant matter. When these plants uptake carbon from the atmosphere, it is stored until they are burned or used as feedstock for biodiesel production. Thus, the combustion of this biodiesel only returns the carbon the plants took out of the atmosphere initially [30].

The main problems that prevent the direct use of the raw waste cooking oils in different combustion systems are its high molecular weight, high viscosity and low volatility which lead to poor atomization in the combustion chamber [31]. The conversion of raw waste cooking oils into biodiesel is an efficient way to overcome these problems. Pyrolysis, emulsification, and transesterification are the popular techniques used to produce biodiesel. However, the use of transesterification is the most common economic and effective technique.

2.2.1 Transesterification reaction

In the transesterification process, the triglyceride molecules of vegetable oils are converted into smaller, straight chain molecules (almost similar in size to the molecules of the species present in diesel fuel). Figure 2-4 shows transesterification schematic representation.

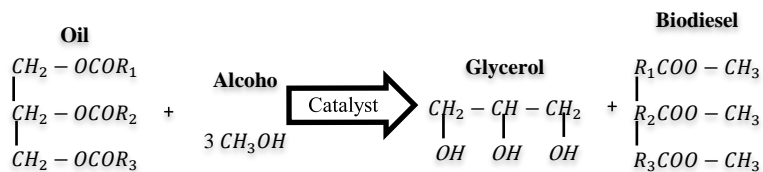


Figure 2-4 Stoichiometric transesterification reaction

The following subsections represent the main parameters affecting the transesterification reaction of biodiesel and then review about the biodiesel production researches via transesterification of vegetable oils will be stated.

2.2.2 The parameters affecting the transesterification reaction

Transesterification is the reaction of triglyceride molecules of vegetable oils and alcohol to produce esters and glycerol. The most critical parameters that influence the transesterification reaction time and conversion are: -

- **Catalyst type and concentration**

Alkalis, acids, or enzymes can catalyze the biodiesel in the transesterification reaction. Alkali-catalyzed (NaOH, KOH) is the most commonly used in the transesterification reaction of waste cooking oil as it is much faster than acid-catalyzed (HCl, H₂SO₄) transesterification [32].

Attia and Hassaneen. [33] investigated biodiesel production from waste cooking oils with different base catalysts (NaOH, KOH). They also evaluated the effects of the catalyst weight (0.5% and 1%). The optimum condition that produced the highest yield around 96% was 60°C reaction temperature, 1% wt/wt KOH catalyst and 6:1 molar ratio of methanol to oil. The KOH show 4% higher conversion in comparison with NaOH.

Refaat et al. [34] investigated biodiesel production from waste cooking oil with KOH and NaOH as a catalyst with different concentrations (0.5% and 1%) by weight. The optimum condition that produced the highest yield around 98.16% was 65°C reaction temperature, 1% wt/wt KOH catalyst and the molar ratio of 6:1 of methanol to oil. The KOH show 1% high conversion in comparison with NaOH.

The increase of catalyst concentration has an adverse impact on the product yield as any excess amount of alkali catalyst reacts with triglycerides to form more soap [35].

- **Mixing intensity**

Mixing plays a great role in the transesterification reaction as oil and methanol are immiscible [36]. Ultrasonic sound waves with low frequency is an efficient mean to generate proper mixing. It can significantly reduce the reaction time to accelerate biodiesel production process. Ultrasonic waves main effect on chemical reactions comes from the formation and collapse of microbubbles that improves the mass transfer by disrupting the interfacial boundary layers [37].

Kumar et al. [38] had successfully conducted that presence of ultrasonic irradiation (50% amplitude, 0.7 s cycle each second) enhanced the kinetic rate of transesterification of *Jatropha curcus* oil, with a reduced reaction time to 15 min compared to 6 h of conventional processing time with an obtained yield of 98%. Samani et al. [39] found that pistachio biodiesel conversion (yield) in the biodiesel produced by the ultrasonic system was 7.5 times greater than that of the conventional method.

- **Alcohol to oil molar ratio and alcohol type**

One of the most critical variables affecting the biodiesel (alcohol ester) yield is the molar ratio of alcohol to oil (triglyceride). The stoichiometric molar ratio of alcohol to triglycerides is 3:1 which yield three moles of fatty acid alkyl esters and one mole of glycerol. However, an excess amount of alcohol is required to ensure the completeness of the transesterification reaction; as the

conversion reaction is reversible so additional value is needed to get complete conversion of the raw oil. Many researchers confirm that maximum conversion to the ester occurs at a molar ratio of 6:1 [33].

Methanol and ethanol are the most common alcohols used in the transesterification reaction. They are not miscible with triglycerides at ambient temperature, so the mixing is essential to enhance the mass transfer. Most of the Egyptian researchers prefer to use methanol due to its availability and its low cost.

- **Reaction temperature**

The reaction temperature affects the yield of biodiesel. As the reaction temperature is increased, the biodiesel conversion rate increases and the reaction time decreases because of the reduction of oils viscosity. However, that increase in reaction temperature more than the optimal value leads to deterioration of biodiesel yield, because the saponification of triglycerides increases at the higher reaction temperature. To prevent the alcohol evaporation during transesterification reaction, the temperature should not exceed the alcohol boiling temperature. Usually, the optimal reaction temperature range is from 50°C to 65°C [35].

2.3 Gas Turbine Emissions

Gas turbine engines in addition to diesel generators, emit undesirable emissions. The most regulated air pollutants include nitrogen oxides (NO_x) and carbon monoxide (CO). The following sub-section covers the definition, formation mechanism, and reduction methods of gas turbine emissions, mainly CO and NO_x emissions.

2.3.1 Carbon monoxide (CO)

CO the major intermediate species before complete oxidation of carbon contents into CO_2 during the combustion of hydrocarbon fuels. As such, hydrocarbon fuels first are broken down and form a substantial amount of CO then the oxidation of CO to CO_2 occurs later. CO can be produced due to many reasons; including:

- the inadequate O_2 in rich combustion as in diffusion combustion.
- the low temperature of lean combustion, where OH radical (the determining factor in the oxidation of CO to form CO_2) is limited (this active radical is produced when the temperature is greater than 1100 K) [40].
- the high temperature that tends to increase the produced CO due to the dissociation reaction of CO_2 to form CO.

Thus, reduction of CO emissions can be achieved by complete oxidation rate of carbon to carbon dioxide which can be attained with increasing flame temperature, increasing the available oxygen, increasing the combustion pressure, and lengthening the residence time to achieve the equilibrium of CO also with ensuring good mixing to eliminate local rich zones and so decreasing the CO formation.

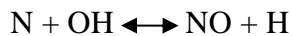
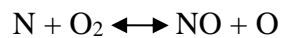
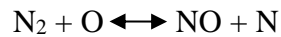
2.3.2 Nitrogen oxides (NO_x)

NO_x is the term comprising both gases of nitric oxide (NO) and nitrogen dioxide (NO_2). NO is mainly formed in a combustion process due to high temperature (>1850 K), the long residence time in the reaction zone and high

pressure [11]. NO₂ is formed by oxidation of NO in the lean combustion conditions at low temperature. Generally, the concentration of NO₂ is lower than that of NO because the rate of the oxidation of NO is too slow to give significant conversion in short residence time. In order to control the formation of NO_x emissions, the various mechanisms of NO_x formation should be well understood. There are three major mechanisms to produce NO_x: thermal NO_x (Zeldovich mechanism) [11], fuel NO_x and prompt NO_x (Fenimore) [41].

- **Thermal NO_x (Zeldovich mechanism)**

Thermal NO_x is an endothermic reaction producing NO and the significant rate can be produced only at temperatures above 1850 K due to the high activation energy required to initiate the oxidation of nitrogen (first reaction). The extended Zeldovich mechanism consists of three principal reactions controlling the production of thermal NO_x:



To control the thermal NO_x, the combustor should operate at a low temperature that can be achieved at lean conditions i.e. low equivalence ratio as thermal NO_x is mainly depended on the flame temperature which is decreased by decreasing the combustor equivalence ratio.

- **Prompt NO_x (Fenimore)**

The prompt NO is produced from the rapid reaction of atmospheric nitrogen (N₂), with short-lived hydrocarbon radicals such as C, CH, and CH₂ in the

reaction zone at low temperature (below 1000 K) [40]. The prompt NO can be ignored under lean combustion conditions due to the reduced hydrocarbon radical concentration.

- **Fuel NO_x**

Most fossil fuels especially coal contain small amounts of fuel bound nitrogen which can form fuel NO_x. The fuel NO_x results from the oxidation of the nitrogen contained in the fuel. The significant rate can be produced only when the combustor operates at rich conditions using fuel having a large fraction of nitrogen compounds. The liquid and gases fuels used in gas turbine combustion contain approximately no fuel bound nitrogen as compared to solid fuels and hence fuel NO_x is ignored.

2.4 Emissions Characteristics for Biodiesel in Gas Turbines

There are a lot of researchers who focused on the investigation of combustion and emission characteristics of biodiesel in gas turbines; as collected in Table 2-2. This table shows selected studies related mainly to the adoption of the LPP concept in gas turbine applications using conventional fuel (Jet A-1 or diesel), biodiesel and blends of Jet A1 and/or diesel with biodiesel. The latter is obtained from different renewable sources including Jojoba methyl ester (JME), Palm Methyl Ester (PME), Jatropha Pure Oil (JAPO), Jatropha Methyl Ester (JAME), Soy Methyl Ester (SME), Canola Methyl Ester (CME) and Rapeseed Methyl Ester (RME). There were no detected studies where WCOME was studied, so other biodiesels (characterized by oxygen contents as that of WCOME) were noticed to explore the impact of biodiesel on gas turbine emissions. It can be concluded that the use of biodiesel and its blends

with fossil fuels in gas turbine combustors would be more effective for the reduction of CO and NO_x emissions.

Lean Pre-vaporized Premixed (LPP) concept introduces a promising solution to meet the purpose of reducing NO_x emissions as well as other pollutants [11]. In this concept, the liquid fuels are burned via premixed combustion rather than diffusion combustion and so the corresponding complexities in diffusion flames are removed. However, LPP combustion suffers from a number of problems such as combustion instabilities ([42] and [43]). Providing the combustor with a swirling flow commonly enhances the LPP flame stability [44]. The emission characteristics of LPP combustion depend on the flow field, fuel evaporation and the fuel/air mixing quality [45].

Table 2-2 Selected previous studies related to biodiesel emission in gas turbine applications

Reference	Test Conditions	Findings
Gokulakrishnan et al. [46]	<ul style="list-style-type: none"> ○ Fuel oils, ○ High pressure, ○ Swirl-stabilized LPP combustion system 	<ul style="list-style-type: none"> ● Fuel oils achieved very low NO_x emissions comparable to those of natural gas in a lean premixed combustion system.
Attia et al. [47]	<ul style="list-style-type: none"> ○ Jet A-1 fuel ○ Blends of Jet A-1 with jojoba methyl ester (JME) fuel ○ LPP swirl-stabilized combustion test rig ○ $\phi=0.87$ ○ SN=0.78. ○ Combustor inlet temperature =170°C. 	<ul style="list-style-type: none"> ● As the blending ratio of JME increases the NO_x emissions decrease. ● The CO emission is higher than that of the Jet A-1 fuel by approximately 0.15 % at the end of the test section.

Reference	Test Conditions	Findings
<p>Hashimoto et al [48]</p>	<ul style="list-style-type: none"> ○ Atmospheric pressure ○ Palm Methyl Ester (PME) ○ Atmospheric pressure ○ Air Preheating Temperature = 400°C. 	<ul style="list-style-type: none"> ● For excess air ratio of 2.53, the NO_x emissions for PME were lower compared to diesel under the same operating conditions. ● The CO emissions were comparable for both fuels.
<p>Hashimoto et al [49]</p>	<ul style="list-style-type: none"> ○ Jatropha Pure Oil (JAPO) ○ Jatropha Methyl Ester (JAME) 	<ul style="list-style-type: none"> ● CO emissions for the pure oil were higher than those of diesel and JAME, especially at a low adiabatic flame temperature. ● NO_x emissions were comparable for all the tested fuels, especially at fixed air flow rates.
<p>Habib et al [50]</p>	<ul style="list-style-type: none"> ● Fuel: <ul style="list-style-type: none"> - Jet A - Soy Methyl Ester (SME) - Canola Methyl Ester (CME), - Rapeseed Methyl Ester (RME), - Blends: <ul style="list-style-type: none"> - B50 (i.e. blends containing 50% of Jet A and 50% of biodiesel on the volume basis) 	<ul style="list-style-type: none"> ● The biodiesel and biodiesel Jet A blends reduced the CO and NO_x emissions emitted from the turbine.

2.5 Research Aims

From the previous literature review it can be concluded that the LPP system can be tested under different conditions (including fuel type, preheat

temperature, and mixture strength) and it has a great remarkable positive effect on NO_x and CO reduction in addition to its enhanced combustion efficiency. However, there were few studies conducted to investigate the combustion performance of liquid biofuels using a swirl stabilized LPP technique, with rare investigations where biofuel produced from waste cooking oil was studied. Biodiesel addition to fossil liquid fuels has a great ability to reduce gas turbines toxic emissions. There was no work at least in Author's hand where LSB and HSB having the same SN were compared.

Based on these conclusions the main objective of the present study is to investigate the influence of WCOME blending ratio on the combustion characteristics of swirled stabilized LPP flames of blended fuels. This objective can be realized by achieving the following tasks:

1. Design and manufacture of two swirl burners having identical swirl number and different swirl flow configurations.
2. Compare the cold flow, the combustion and the emissions characteristics for the previous burners using LPP combustion.
3. Produce biodiesel from waste cooking oil to get WCOME following the transesterification process using ultrasonic waves.
4. Study the combustion characteristics of different blends of Jet A-1 and WCOME on the combustion and emission characteristics of swirl stabilized LPP combustion.
5. Compare the Jet A-1 / WCOME blends with that of the reference fuel (Jet A-1) using swirl stabilized LPP combustion.

Chapter 3: TEST FACILITY AND PROCEDURE

This chapter describes the experimental setup and the measuring techniques used in this study. In the first part of the chapter, the biodiesel production procedures via transesterification reaction are discussed. Then the biodiesel evaluation is performed. Finally, the physical and chemical properties of the produced biodiesel are determined following the corresponding standard tests methods. In the second part of this chapter, the components of the combustion test facility are described in detail. Then the measuring instruments used to determine the cold flow, flame temperature and species concentrations are briefly discussed. Finally, test procedure and data analysis are formulated.

3.1 Biodiesel Production Procedures

In this study waste cooking oil collected from fast food restaurants has been considered as feedstock for biodiesel production. The technical specifications of the received raw oil after its filtration and cleaning from suspended materials are listed in Table 3-1.

Table 3-1 Technical specifications of the used raw waste cooking oil

Fuel Property	Value
Density @ 15°C, kg/m ³	0.93
Kinematic viscosity @40°C, mm ² /s	40.3
Flashpoint °C	200
Pour point °C	15
Water content (%)	0.5
Higher heating value (MJ/kg)	35.5
Cetane number	42

Transesterification process has been used to convert waste cooking oil into biodiesel. In the current study, the used base catalyst is potassium hydroxide

(KOH), and the alcohol is methanol. The major steps to produce biodiesel using ultrasonic transesterification are shown in Figure 3-1. Based on the review of the previous researches the following procedures are conducted to perform the transesterification.

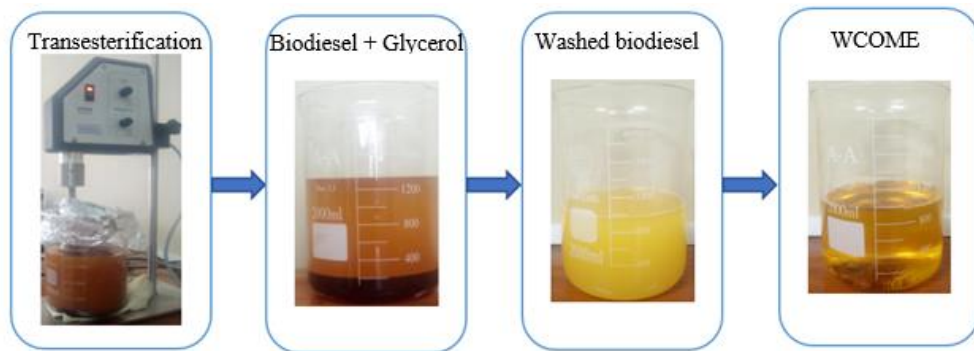


Figure 3-1 Major steps to produce biodiesel using ultrasonic waves

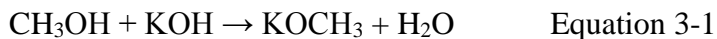
- **Pretreatment of waste cooking oil**

The pretreatment stage is divided into two steps. The first one is the filtration process. The collected waste cooking oil should be heated up to reduce the high viscosity of WCO which almost loses its flow characteristics below 15°C. Then oil is filtered to remove dirt, charred food, and other non-oil material found. The second step is moisture removal by preheating the waste cooking oil to 120°C for 15 min which let the water contents within oil to evaporate. Then oil is allowed to be cooled naturally.

- **Transesterification reaction**

The experiment was carried out in a 2 liters flask. A mixture of 330 ml of methanol and 1% wt. KOH was agitated using a magnetic stirrer (IKA C-MAG

HS 7) for 5 min to form potassium methoxide and water according to the following reactions.



Then, 1 liter of raw waste cooking oil was heated to 65°C by using a hot plate controlled by (IKA ETS D-5) temperature controller. After that, the hot oil was mixed with the previously prepared potassium methoxide. Afterward, the mixture was transferred to be subjected to ultrasonic waves for 15 min. Ultrasonic irradiation was provided by a UP200S Hielscher as shown in Figure 3-2.



Figure 3-2 Ultrasonic setup

- **Biodiesel and glycerin separation**

Once the reaction is completed, the oil is transferred to a settling vessel for 2-3 hours, where the biodiesel and glycerol byproduct settled and separated. The density difference between these liquids is a dominant parameter in the separation process. The glycerol is drawn-off from the bottom of the settling vessel by gravity force. The settling and separation process is shown in Figure 3-3.

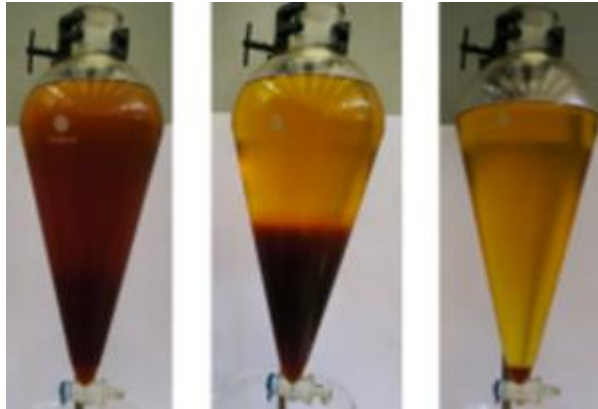


Figure 3-3 Settling and separation process

- **Biodiesel washing and drying**

Biodiesel washing process follows the glycerol separation process to remove any residual components within the biodiesel fuel, mainly excess methanol and soap content. This process is repeated many times (2-3) to have completely clean biodiesel as shown in Figure 3-4. The washing is accomplished by using warm potable water at 50°C. The washed biodiesel then dried by increasing its temperature to 120°C. The clean biodiesel is shown in Figure 3-5.



Figure 3-4 Water washing process



Figure 3-5 Waste cooking oil biodiesel

3.2 Produced Biodiesel Evaluation

The quality of the biodiesel preparation process can be evaluated according to the physical and chemical properties of the biodiesel and the product yield which is defined as the percentage volume of the final product (biodiesel) relative to the volume of raw oil. In the current experiment, the product yield was 98%. The following part of the chapter will concern with the evaluation of physico-chemical properties of the prepared biodiesel at the Advanced Testing Lab for Measurements of Environment and Biofuel funded by STDF at Benha Faculty of Engineering. including the flash point, density, viscosity, heating value, elemental analysis, and thermogravimetric analysis.

- **Biodiesel thermogravimetric analysis**

The thermogravimetric analysis (TGA) measures the amount and rate of mass change of a material as a function of the increased temperature. This analysis is used in the current study as an indication of fuels volatility with the help of Labsys Evo-Setaram analyzer shown in Figure 3-6. In this test, a fuel sample was put in alumina crucible of the capacity of 440 μl and the fuel quantity was measured by Mettler Toledo X6 sensitive balance (with an accuracy of $\pm 1 \mu\text{g}$).

The temperature was increased from 25 to 550 °C with a heating rate of 15 °C/min in an atmosphere of argon supplied at the rate of 200 ml/min. The weight loss percentage of the sample was monitored throughout the heating process; as shown in Figure 3-7 where TGA for raw waste cooking and WCOME are provided.

It is observed that the mass of the biodiesel starts to decrease approximately at a temperature higher than 250°C, and it continues decreasing until all the biodiesel is almost vaporized. Similarly, evaporation of raw waste cooking oil starts approximately at 400°C and ends at about 475°C. Thus, the transesterification process enhanced the volatility characteristics of the produced WCOME.



Figure 3-6 Thermal analyzer setup

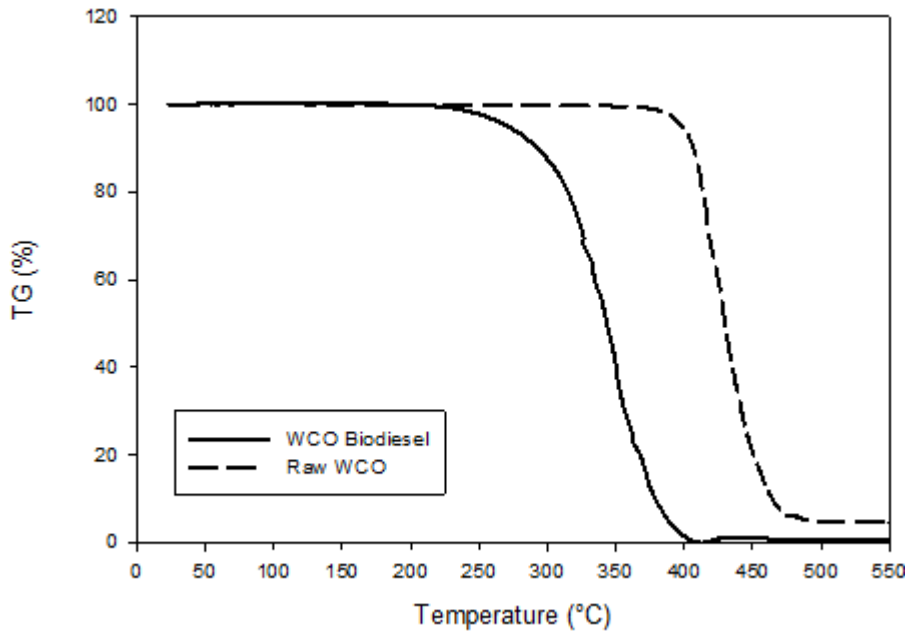


Figure 3-7 The thermogravimetric analysis of WCOME B100 and raw WCO

- **Elemental analyzer (EA)**

The Euro Vector EA3000 of CHNS-O Elemental Analyzers, shown in Figure 3-8, with its dedicated software Callidus, is used to determine Carbon, Nitrogen, Hydrogen, and Sulphur mass fraction in the biodiesel and raw waste cooking oil. This is achieved through the combustion of the sample in a tin crucible at a reactor packed with electrolytic copper and copper oxide at a temperature of 980°C, and the resultant gaseous species (N₂, CO₂, H₂O, and SO₂) are analyzed using a thermal conductivity detector (TCD).



Figure 3-8 Elemental analyzer setup

The physicochemical properties of the prepared WCOME compared to those of Jet A-1 are shown in Table 3-2. The main properties of WCOME meet the ASTM requirements. The main differences for those of WCOME over those of Jet A-1 include 10% higher density, more than 4 times higher viscosity, 3.5 times higher flash point and twice molecular weight values, 8% lower heating value, slight lower carbon/hydrogen ratio, and oxygen contents of 11% on mass base. These properties indicate that the atomization of WCOME is poorer than that of Jet A-1 leading to the formation of larger fuel droplets having a higher boiling time. Thus, the use of higher portions of WCOME will lead to partially premixed rather than fully premixed combustion.

Table 3-2 Properties of the used fuels, Jet A-1 and waste cooking oil biodiesel

Property	Test method	Jet A-1	WCOME
Specific gravity at 15°C	ASTM D-1298	0.797	0.877
Viscosity at 40°C, cSt	ASTM D-445	1.08	4.53
Pour Point °C	ASTM D-97	-43	-6
Flash Point °C	ASTM D-93	39	130
Boiling point °C at 1 atm	ASTM D-86	163	350
Lower calorific value, MJ/kg	ASTM D-240	43.465	39.98

Property	Test method	Jet A-1	WCOME
Molecular weight, kg/kmol	-	148.025	290.914
Elemental analysis, % by mass:			
Carbon		86.51	77.22
Hydrogen	Euro Vector EA3000	13.48	11.46
Sulfur	CHNS/O Elemental	Nil	Nil
Oxygen	Analyzer	Nil	11.3
Nitrogen		Nil	Nil

3.3 The Combustion Test Rig

The experiments are conducted using swirl stabilized lean pre-vaporized premixed (LPP) combustion test rig in continuous combustion laboratory, Mechanical Power Department, Benha Faculty of Engineering, Benha University, Egypt. The combustion chamber is opened to the atmosphere and thus, all tests are made at atmospheric pressure. The schematic diagram of the experimental test rig is illustrated in Figure 3-9. The major components of the current test facility are the air delivery system, air heating system, fuel supply system, swirl-stabilized burner, and the combustion chamber. The following sub-sections provide more details about the experimental apparatus used.

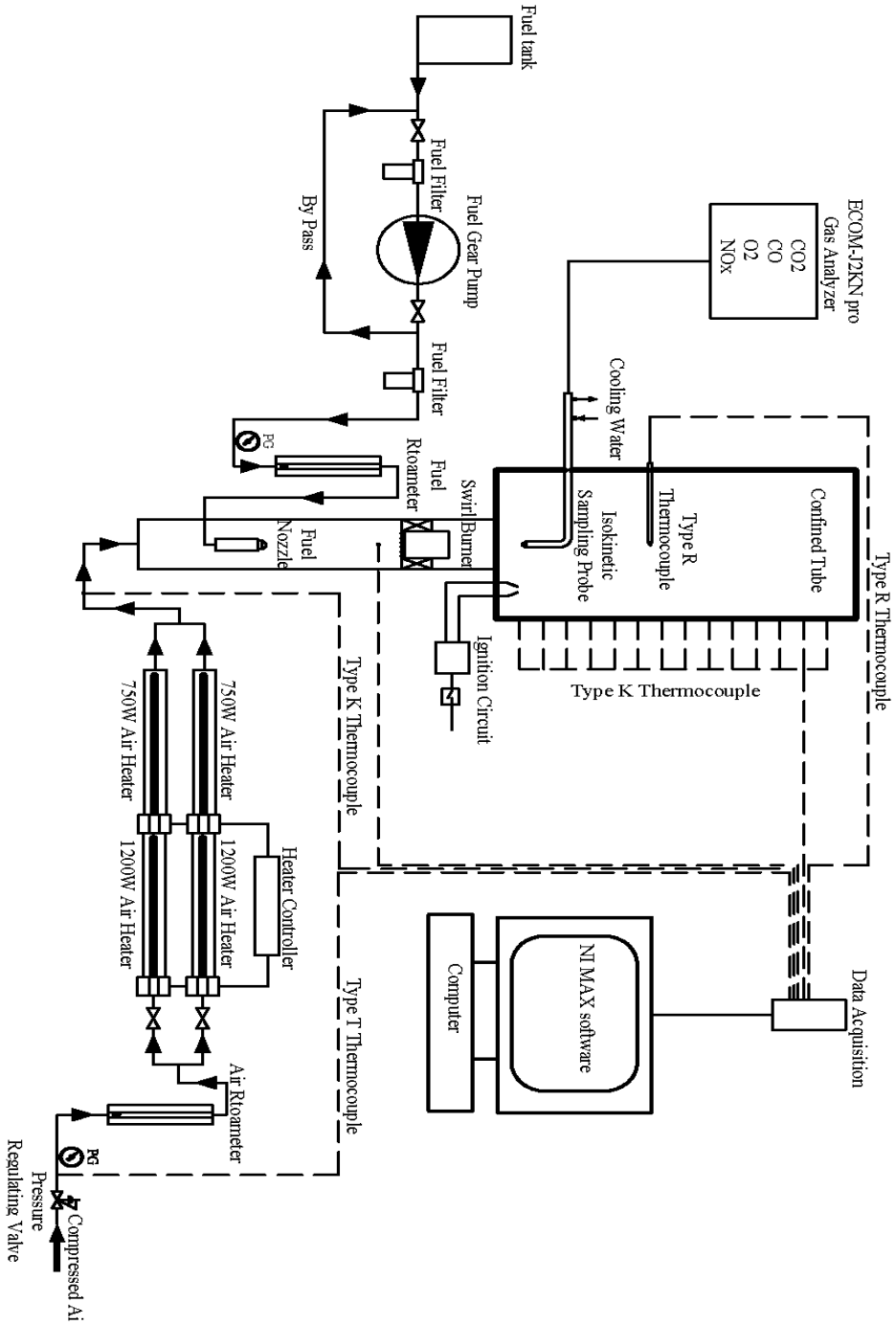


Figure 3-9 Test rig schematic drawings

3.3.1 Combustor and swirl burners

The combustor used in this study is a simple vertical confined steel tube with 150 mm internal diameter and 500 mm length as shown in Figure 3-10. The tip of the burner is aligned with the dump plan of the combustor. The flame is ignited by means of an electrical ignition circuit consists of two steel electrodes and a high voltage transformer. The detailed discussion regarding the selection of the current combustor dimensions is stated by El-Zoheiry [51]. The combustor tube is provided with a longitudinal groove to facilitate measurement of local concentration and local temperature at specific radial and axial positions. The combustor exit was opened directly to the atmosphere without any restrictions.

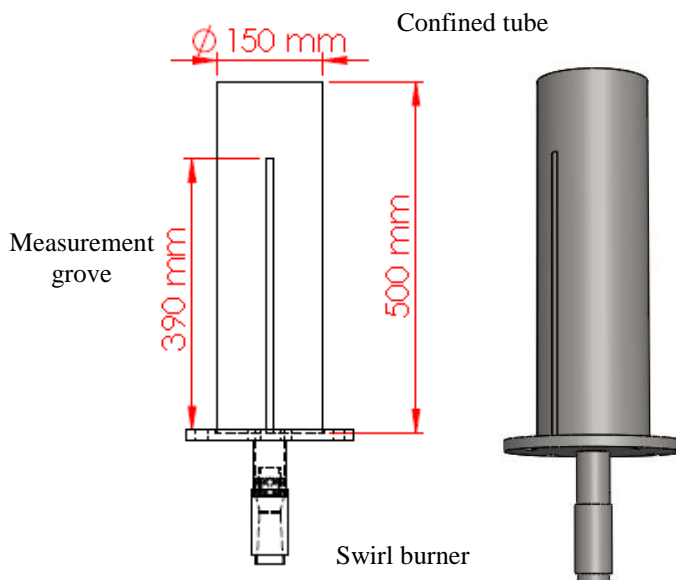


Figure 3-10 The LPP Combustor

The swirl burners used in the current study are illustrated in Figure 3-11; including HSB and LSB. The HSB consists of 8 straight fixed axial vanes with 1.25 mm thickness attached to the outer surface of a center body with a discharge angle $\theta = 35^\circ$ relative to the incoming flow. The HSB has outer annular and center bluffbody radius of $R_b = 21.5$ mm and $R_c = 11.2$ mm, respectively. The swirl lengths is $L_s = 26$ mm. The corresponding geometric swirl number is calculated using Equation 2-1 in this case $S_N = 0.55$.

The LSB has outer annular and center channel radius of $R_b = 21.5$ mm and $R_c = 13.5$ mm, respectively, with the ratio of $R = 0.628$. The channel and the swirl lengths are $L_c = 13.5$ mm and $L_s = 26$ mm, respectively. The LSB has 8 straight axial vanes mounted around the central channel with a discharge angle of $\theta = 40^\circ$ relative to the incoming flow. The blockage ratio of the center straight flow is controlled by a perforated plate has a diameter of 27 mm and 5 mm thickness. It is provided with 40 holes of 3 mm diameter arranged in a circular pattern. The corresponding swirl number is calculated using Equation 2-2 in this case $S_N = 0.55$.

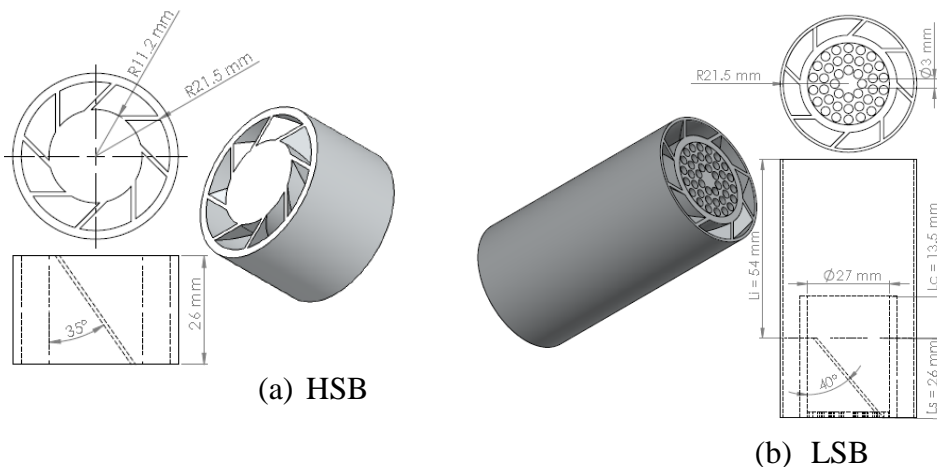


Figure 3-11 The configurations of the present HSB and LSB

Table 3-3 Geometric dimensions of the present HSB and LSB

Parameters	HSB	LSB
SN	0.55	0.55
θ	35°	40°
n	8	8
L_i	-	54 mm
L_s	26 mm	26 mm
L_c	-	13.5 mm
R	0.521	0.628

3.3.2 Air delivery system

A screw compressor supplies air to a pressure accumulator tank of 2 m³ capacity. The accumulator tank is kept at relatively constant pressure between 9 bar to 10 bar. A pressure regulating valve is installed after the tank and before the air enters the test facility to provide a constant supply pressure and to eliminate the air flow fluctuation. The pressure regulating valve can change the pressure from 0 to 10 bar. During the experiments the pressure is adjusted to 10 bar to match the requirements of other elements in the whole test facility.

The actual air volume flow rate during operation is measured using a Dwyer high flow glass rotameter (Model DR41404 of flow range from 1 to 16 CFM i.e. 1.7 to 27.2 m³/hr.). The air pressure is measured by means of a pressure gauge installed after the pressure regulating valve to calculate air density. The air inlet temperature is measured by thermocouple type T connected with DAQ. Figure 3-12 shows the main components of the air delivery system.



(a) Screw compressor

(b) Regulator

(c) Rotameter

Figure 3-12 The main components of the air delivery system.

3.3.3 Air heating system

A set of four process air inline heaters are used to preheat the air entering the system from room temperature up to above the Jet A-1 fuel boiling point. This preheat temperature is monitored using K-type thermocouples at the heaters exit in conjunction with the data acquisition card. The air heaters outlet temperature is controlled using two variable autotransformers. The variable autotransformers supply the heaters with the predefined power as a function of the inlet voltage for fixed resistance of heaters. A pressure switch is installed on the air line before the heaters to protect the heaters from no flow operating conditions. The pressure switch and the contactor are responsible for automatically disconnecting the power from heaters in case of no air flow. Additional specifications about the used equipment in the air heating system are presented in Table 3-4.

Table 3-4 Specifications of the devices used in the air heating system

Sn.	Device	Model	Specifications
1-	Inline air heaters	Omega AHPF-122	- 240 V - 1200 W - Max CFM is 15
2-	Inline air heaters	Omega AHP-7562	- 240 V - 750 W - Max CFM is 20
3-	Variable autotransformer	SEIDEN	- Ampere range is (0-8 A) - Voltage range (0-240 V)
4-	Pressure switch	Euroswitch NO model 4111122DI	- Pressure range (0-10 bar) - Tolerance (0.1 bar)

3.3.4 Fuel supply system

The fuel is pumped from a scaled beaker of two liters capacity using fuel pump model (SUNTEC-AL Oil Pump of pressure range from 1-25 bar). The fuel line is provided with two fuel filters. The first one is located before the pump and the other before the fuel flow meter. Filters are employed to protect the fuel pump and flow meter from blockage due to any impurities in fuel or in fuel line. A pressure gauge is installed to monitor the pressure after the pump. The fuel volume flow rate during operation is measured using a Dwyer high flow glass rotameter (Model DR224632). The pressurized fuel is injected via a pressure atomizer inside the mixing steel pipe. The fuel injector consisted of the nozzle adapter, fuel nozzle, and sintered filter. The fuel nozzle is installed on the nozzle adapter which is made from brass. The main part of the fuel injector is the fuel nozzle which is a single hole nozzle having 1.9 l/h flow rate, and 30° solid spray angle.

3.4 Measuring Instruments

3.4.1 Cold flow measurements

For cold flow measurements, a calibrated L-shape five-hole pressure probe with a tip diameter of 3.18 mm and a 152.4 mm overall length has been used. The five-hole probe is connected with DAQ system to determine the axial, tangential, and radial velocity components. The analysis is performed via Aeroacquire software (version 4.10.2) to obtain the velocity vectors, total and static pressures. The five-hole probe and DAQ system are shown in Figure 3-14. The tip geometry of the five-hole probe and its coordinate system are shown in Figure 3-13 while the flow chart for calculating the velocity components are shown in Figure 3-15. Where P_1 is the pressure measured at the central probe hole, P_2, P_3 are the pressures measured in the pitch plane, P_4, P_5 are the pressures measured in the yaw plane. P_t is the total pressure, P is the static pressure. k_t is the total pressure coefficient, k_s is the static pressure coefficient, k_β is the directional coefficient in pitch plane, and k_α is the directional coefficient in yaw plane.

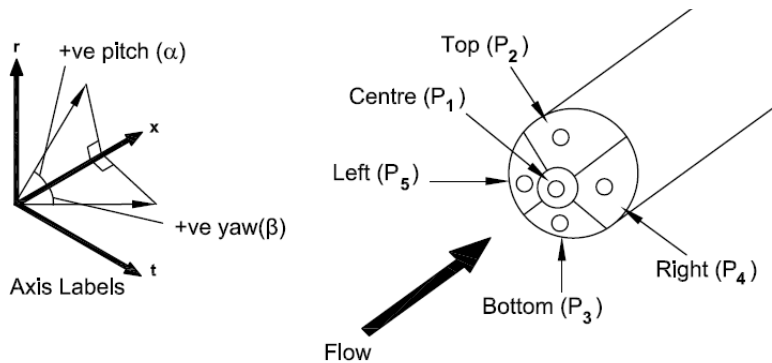


Figure 3-13 The tip geometry of the five-hole probe and its coordinate system

(a) Five-hole pressure probe



(b) DAQ system

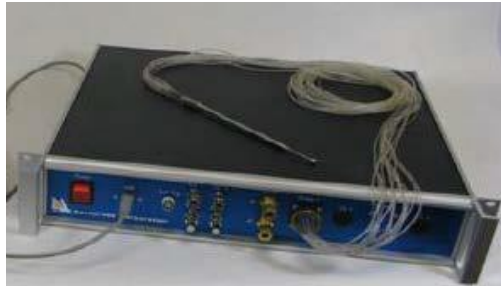


Figure 3-14 Five-hole pressure probe and DAQ system.

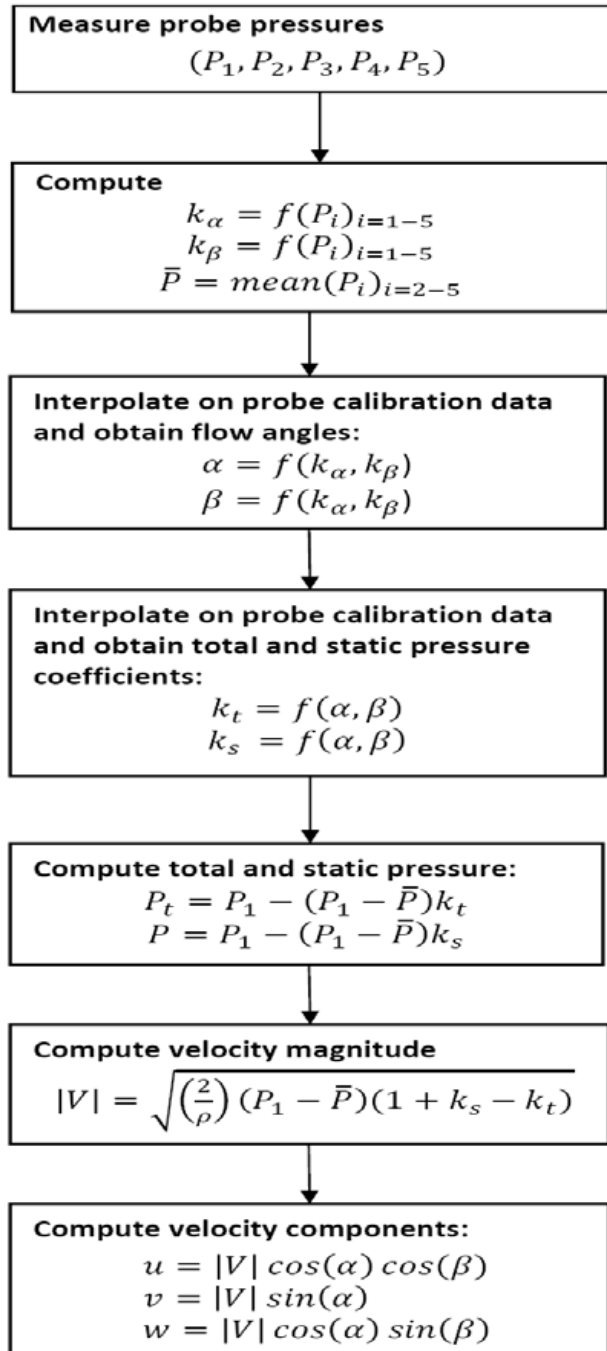


Figure 3-15 The flow chart for calculating the velocity components

3.4.2 Temperature measurements

The temperature measurements were performed using a fine type R (platinum/platinum-13% rhodium) thermocouple with ceramic tube insulation. The thermocouple has 100 μm wire diameter and 0.6 mm bead diameter and accuracy of $\pm 1.5^\circ\text{C}$. The wall temperatures of the combustor are measured at twelve different locations along the combustor wall by calibrated K type thermocouples. The signals of all thermocouples are acquired automatically utilizing Data Acquisition Card Model NI USB-9213 and LabView software.



Figure 3-16 Fine type R (platinum/platinum-13% rhodium) thermocouple.

3.4.3 Species concentrations measurement

The combustion gases are sampled along the combustor axis by a water-cooled stainless steel probe (indirect quenching probe of 8 mm outer diameter) in conjunction with a handheld gas analyzer (ECOM-J2KN Pro). The cell types, measuring range, and accuracy of the emission analyzer for each constituent are illustrated in Table 3-5.

Table 3-5 Resolution and range of gas analyzer for emission concentrations

Gas emission	Measuring range	Resolution	Uncertainty	Principle
O ₂	21 vol. %	0.1 vol. %	0.48%	Electrochemistry
CO ₂	0 ... 20 vol. %	0.1 vol. %	0.5%	Infrared
CO	0 ... 6.3 vol. %	0.01 vol. %	0.16%	Infrared
NO	0 ... 5000 ppm	1 ppm	0.02%	Electrochemistry
NO ₂	0 ... 1000 ppm	1 ppm	0.1%	Electrochemistry



Figure 3-17 Gas analyzer

3.5 Experimental Program and Procedures

This section describes the procedures used to perform a complete experiment; including measurement of cold flow field velocities using five-hole probe, flame temperature measurement using a thermocouple and species concentrations measurement using the gas analyzer.

For the cold flow field measurements the air flow rate is adjusted using the pressure regulator valve then the L-shape five-hole pressure probe with DAQ system is used to map the combustor velocity distribution. The proper location has been regulated using 2-D traverse mechanism with accuracy of ± 1 mm. During this set of experiment, the air was not preheated and there was no fuel injection. Here the volume fuel flow rate was compensated by using an additional amount of air to keep the same volume flow rate of the premixed reactant used through the current study (where equivalence ratio is kept constant).

For system operation during the combustion measurements (both temperature and species measurements) the following procedure is followed:

1. Adjust the air flow rate using the pressure regulator valve.

2. set heaters supply voltage to obtain the predefined air temperature and enough warm-up time (one hour) to reach a thermal steady state condition indicated by fixed temperature measurements for preheated air and along the combustor wall.
3. Allow fuel injection when the air heaters outlet temperature reaches 150 °C the fuel flow rate is adjusted to keep the equivalence ratio at the specified value using the pump pressure regulator screw then the air fuel mixture is ignited.
4. Start the measurements of flame temperature and species distribution through combustor when fixed air heaters outlet temperature of 250 °C in conjunction with stable the combustor wall temperature is attained. To overcome any disturbances or interference due to existing thermocouple and sampling probe, temperature and species measurements were performed individually.
5. The flame temperature is measured using the type R thermocouples in conjunction with the DAQ. While the combustor wall temperature is measured using the type K thermocouples in conjunction with the DAQ.
6. Warm up the gas analyzer for 30 min. before the measurements and making sure that the sampling probe cooling water is flowing, and suction is provided.
7. Place the five-hole pressure probe (for cold flow measurements), type R thermocouple (for temperature measurement), or sampling probe (for species measurements) on a 2-D traverse mechanism to attain the corresponding distribution of temperature and species in axial and radial directions throughout the combustor. There are ten horizontal plans with vertical distances from the burner tip of 10, 20, 30, 40, 50,

70, 90, 110, 130, and 150 mm. In each plane, the measurements are conducted at nine radial locations with relative radial distance to the burner radius (r/R) from the burner centerline of 0, 0.25, 0.5, 0.75, 1, 1.25, 1.5, 2 and 2.5. The species concentrations and temperature were also measured at the combustor exit ($Z= 500$ mm). A summary of the measurement locations is shown in Figure 3-18.

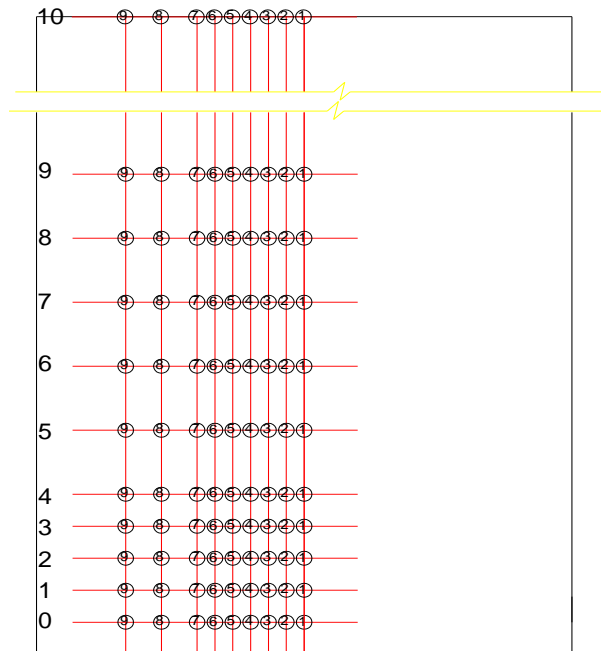


Figure 3-18 Sampling points

3.6 Data Reduction and Analysis

The recorded data for flow velocity, flame temperature, and species concentrations have been processed and analyzed to be normalized or corrected against specific errors.

For cold flow velocity measurements, a sampling rate of 10 sample/sec to collect 1000 readings for each measuring point are time averaged to record the corresponding local mean value.

For flame temperature measurements, 1000 readings with rate of 10 sample/sec are used. The thermocouple readings of the flame temperature are corrected against radiation heat losses by performing an energy balance as expressed by Equation 3-2.

$$h(T - T_{tc}) = \varepsilon\sigma(T_{tc}^4 - T_{sur}^4) \quad \text{Equation 3-2}$$

where T , T_{tc} , and T_{sur} represent the actual temperature, the measuring temperature, and the surrounding temperature respectively, ε is the thermocouple bead emissivity, σ is the Stefan Boltzmann constant (5.67×10^{-8} W/m².K), h is the convection heat transfer coefficient of the surface of the thermocouple. The convection heat transfer coefficient, h , is determined by approximating the thermocouple bead as a sphere with a thermocouple bead diameter $D = 0.6$ mm, the combustion products are calculated by assuming a complete combustion process [52]. Nusselt number (Nu) is calculated from Equation 3-3 for forced convection heat transfer around spherical body [53].

$$Nu = \frac{hD}{k} = 2 + [0.4Re^{1/2} + 0.06Re^{2/3}]Pr^{0.4} \left(\frac{\mu_{\infty}}{\mu_s}\right)^{1/4} \quad \text{Equation 3-3}$$

Where the Reynolds number (Re) and the Prandtl number (Pr) are calculated from Equation 3-4 and Equation 3-5 [53].

$$Re = \frac{\rho VD}{\mu_{\infty}} \quad \text{Equation 3-4}$$

$$Pr = \frac{\mu_{\infty} C_p}{k} \quad \text{Equation 3-5}$$

The properties of the combustion products viscosity (μ_{∞}), thermal conductivity (k), constant pressure specific heat (C_p), and density (ρ) are determined at the adiabatic flame temperature (T_{ad}). On the other hand, the mixture viscosity (μ_s) determined at the thermocouple temperature (T_{tc}) using the Wilke's method [54].

The thermal uniformity through the combustor which can be represented by pattern factor (PF) is calculated for different fuels. PF is one of the parameters that must be considered in the gas turbine combustion [11]. The lower the value of the pattern factor the more the thermal uniformity. PF is calculated using equation 3-6:

$$PF = \frac{T_{max} - T_{mean}}{T_{mean} - T_{in}} \quad \text{Equation 3-6}$$

The average emission index at the combustor exit is calculated for different species. Emission index (EI_i) is a generic way to quantify the level of emissions. The EI for a certain species is defined as the ratio of the mass of the species emitted (i) to the mass of fuel burned and can be calculated according to Equation 3-7 [40].

$$E_{im} = \frac{m_{i,emitted}}{m_{F,burned}} \quad \text{Equation 3-7}$$

The E_i is a dimensionless quantity represented in g/kg fuel to make the species concentration measurement independent of any dilution by air. The level of pollution is also expressed as g/MJ to eliminate the effect of the heating values of different fuels according to Equation 3-8 [40].

$$E_{ie} = \frac{\text{mass of pollutant}}{\text{heat of combustion}} = \frac{E_{im}}{\text{LHV or HHV}} \quad \text{Equation 3-8}$$

The flow velocity, flame temperature, CO, and NO_x distribution are plot using Sigma Plot 12.0 software.

Chapter 4: RESULTS AND DISCUSSION

The experimental program of the present study is introduced in the first section of this chapter. After that, results regarding the behavior of air flowing through different burners have been presented and discussed. Then the experimental results and discussion related to the combustion characteristics of the tested fuels using the LPP combustion system are presented and compared with similar results cited in the literature.

4.1 Experimental Program

The physicochemical properties of fuel used in the current study are illustrated in Table 3-2. The air preheated temperature is kept constant during the current experimental program at 250°C which is higher than the boiling point of Jet A-1 (163°C) and lower than that of the WCOME i.e. the Jet A-1 will be fully evaporated before entering the burner and the mixture, in this case, would be homogeneous and fully premixed. In the case of Jet A-1/ biodiesel blends, the mixture can't be fully evaporated providing heterogeneous and partially premixed combustion. The whole experiments conditions are summarized in Table 4-1.

Table 4-1 Test conditions of experiments

Case sn.	Burner	Fuel type	Air preheating Temperature (°C)	Air flow rate (kg/hr)	Fuel flow rate (kg/hr)	Mixture strength, ϕ	Measured parameters
1	HSB	-	25	25.2	-	-	Cold flow field
2	LSB						

Case sn.	Burner	Fuel type	Air preheating Temperature (°C)	Air flow rate (kg/hr)	Fuel flow rate (kg/hr)	Mixture strength, ϕ	Measured parameters
3	HSB	B0	250	23.98	1.234	0.75	- Temperature -Species concentration
4	LSB						
5	HSB	B5			1.244		
6		B10			1.260		
7		B15			1.268		
8		B20			1.279		

4.2 Effect of Burner Configuration on the Cold Flow Pattern

The flow patterns are evaluated using the cold-flow measurements to understand the air flow behavior within the combustion chamber for both HSB and LSB. The mean upstream velocity of the air exit from the LSB is determined to be 3.75 m/s where no fuel was injected into the air stream; in this part of the study, the amount of pre-vaporized fuel is substituted with additional equivalent volume amount of air. Figure 4-1 shows the measured axial velocity profiles at different axial locations through the combustor for both HSB and LSB versus the radius relative to that of the burner. In the early stage of the combustor, the axial velocity of LSB has its maximum value at the burner centerline and decreases towards the wall. With directing towards the combustor exit away burner tip, the axial velocity declines linearly and becomes more uniform through the radial plane at vertical level $Z = 70$ mm. This behavior may be owing to the fact that, there is a part of air flow injected through axial hole admitting part from the swirling air into the core of combustor and so the region where flow can be recirculated is removed or not dominant. The LSB has no central recirculation zone as confirmed with

findings that achieved by [17,55]. On the other hand, the dominant feature of HSB is a large central recirculation zone downstream of the center body due to the low-pressure region in the core of the burner and the adverse pressure gradients in the radial and axial directions. Moving away from the burner tip, the flow becomes more uniform and the flow is almost uniform beyond level $Z= 50$ mm where the circulation zone is ended. Figure 4-2 shows the normalized axial velocity contours for both burners, where the recirculation zone is clearly observed for HSB.

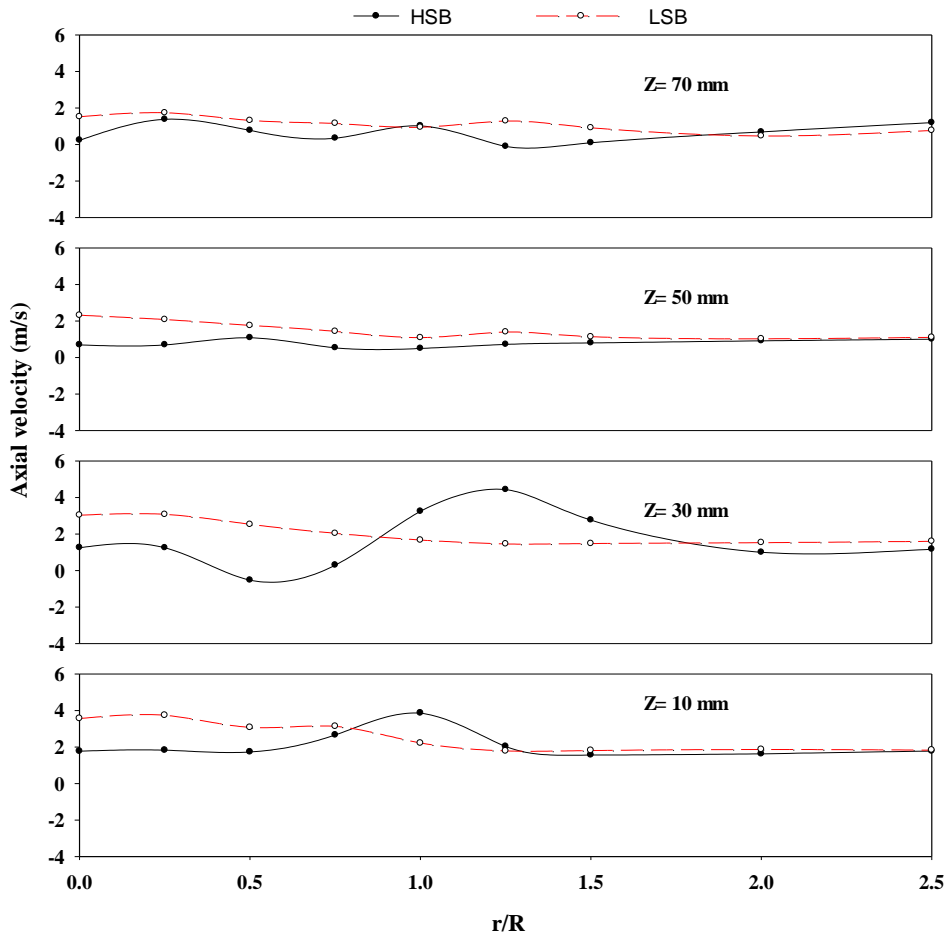
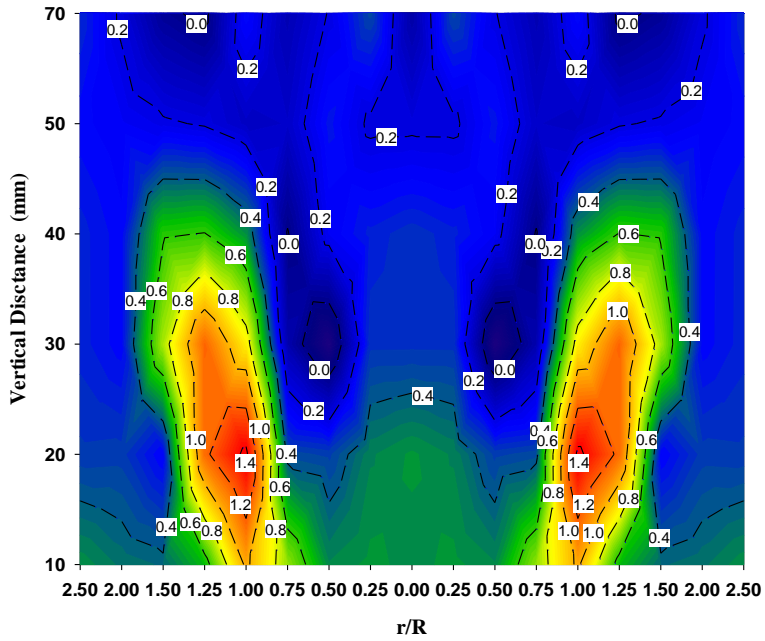
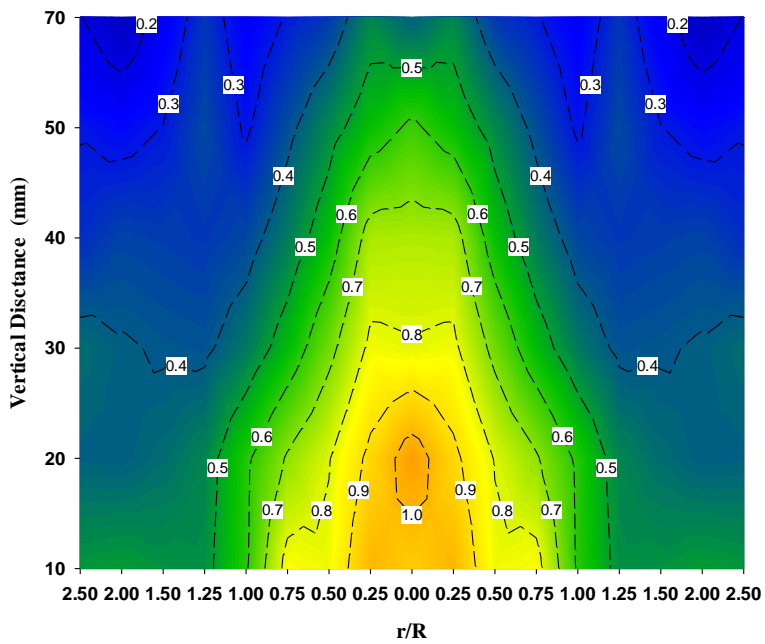


Figure 4-1 Measured axial velocity profiles



(a)



(b)

Figure 4-2 Contours of the normalized axial velocity; (a) HSB and (b) LSB

Figure 4-3 shows the radial velocity at different axial locations through the combustor. The radial velocity distribution reflects the flow homogeneity at each level through the combustor. The radial velocity profile of the HSB shows a higher peak than that of the LSB. It can be noticed that complete uniform flow is attained at $Z=40$ mm for LSB while for the HSB it is achieved beyond $Z= 50$ mm. Levels where the recirculation region are exists have non-uniform velocity. Figure 4-4 shows the normalized radial velocity contours which reflect the lift-off region for LSB and the recirculation zone for HSB. Figure 4-5 shows the total pressure through the combustor for both burners. It can be noted that a low-pressure region is found in the core of the combustor downstream of the HSB and adverse pressure gradients in the radial and axial directions which generate a central recirculation zone downstream of the center body.

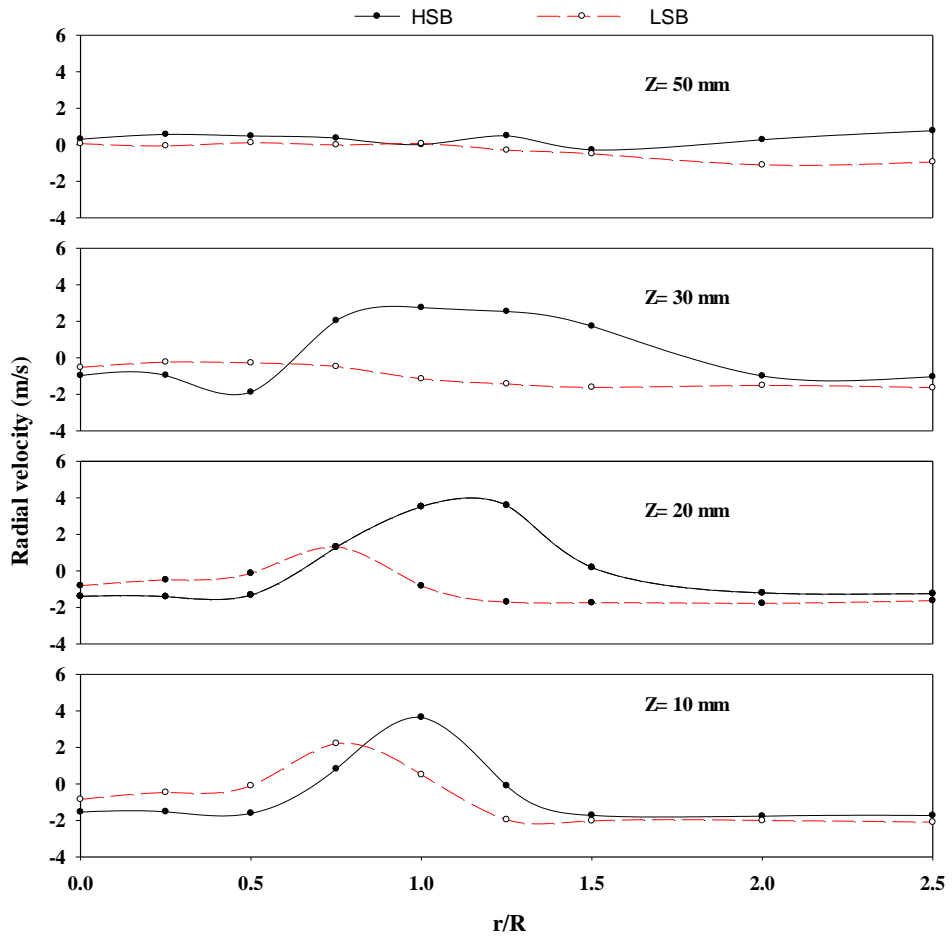
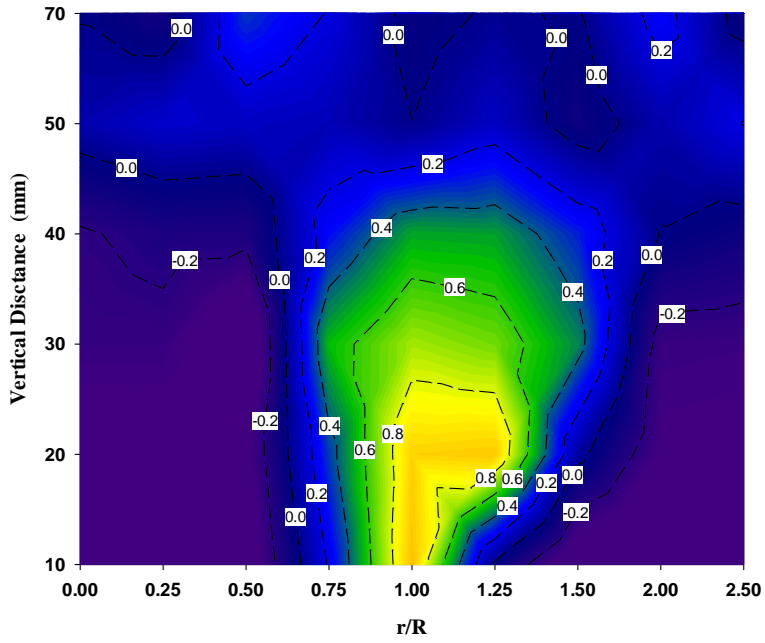
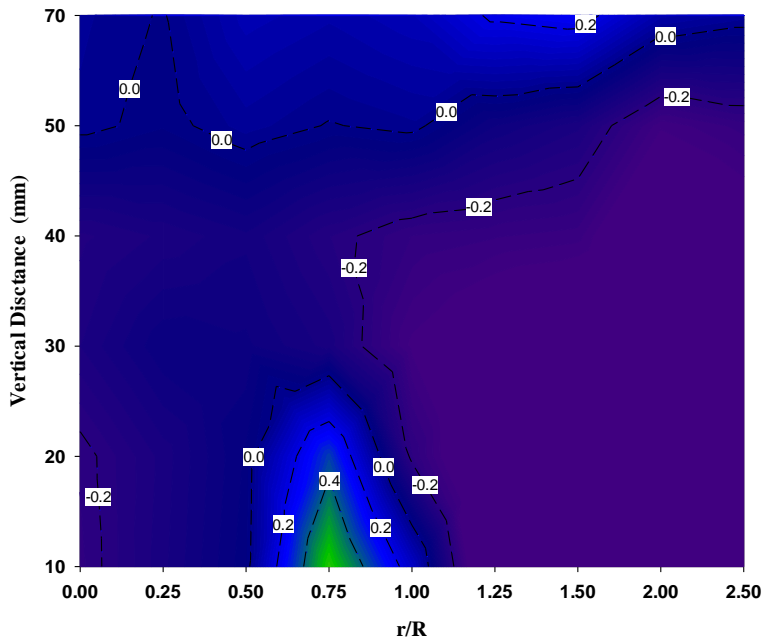


Figure 4-3 Measured radial velocity profiles

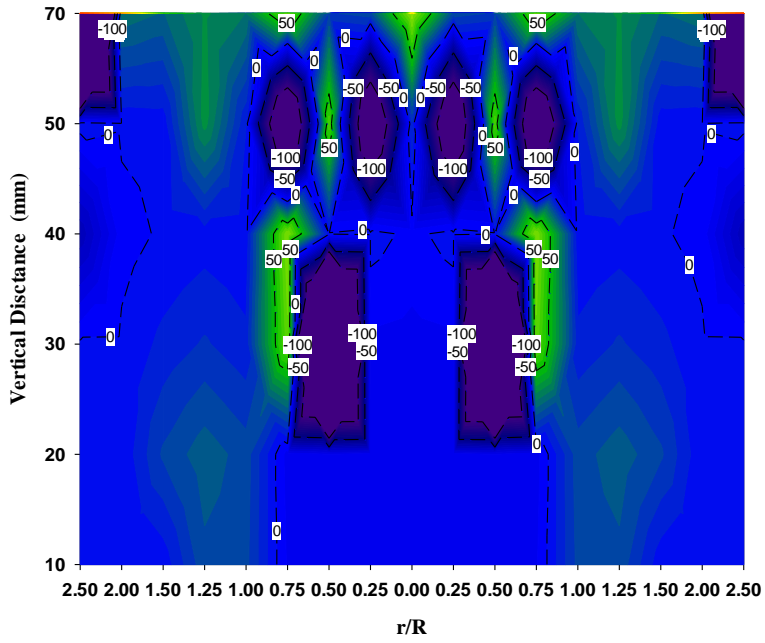


(a)

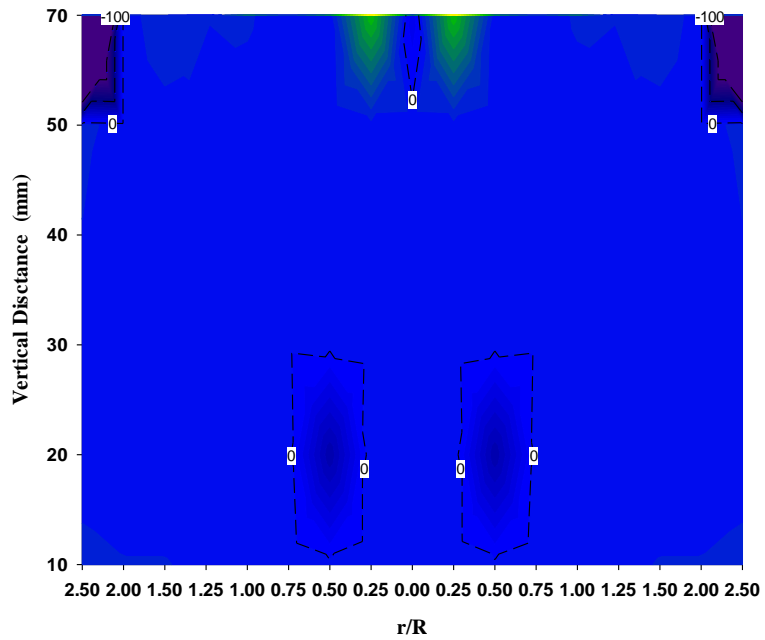


(b)

Figure 4-4 Contours of the normalized radial velocity; (a) HSB and (b) LSB



(a)



(b)

Figure 4-5 Contours of the total pressure (Pa); (a) HSB and (b) LSB

4.3 Effect of Burner Configuration on the Combustion and Emissions Characteristics

The current section represents the combustion characteristics of burning lean premixed mixture of Jet-A1 with air with equivalence ratio of 0.75. These characteristics can be expressed by measuring the exit temperature and the exhaust emissions when two different designed burners having the same swirl number are used as shown in Figure 4-6-Figure 4-8. It can be observed that the mean temperature when HSB is used is higher than that attained when LSB is used. This can be owing to the reduced heat losses from shorter reaction region as resulted from the intensified reactions in the central recirculation zone. The corresponding temperature pattern factor which gives a relative measure of the thermal uniformity of exhaust flow for HSB and LSB are 0.05 and 0.03, respectively. Generally speaking as the flame is lean, the mean values are comparable with slight differences between two burners due to different heat losses along the combustor. Regarding levels of emissions at combustor exit shown in Figure 4-7, it can be noticed that the CO concentrations at the combustor exit plane are more uniform for LSB than for HSB. The mean value of CO at combustor exit is approximately 3 ppm as a result of lean mixture combustion. Figure 4-8 provides the corresponding exhaust NO_x emissions. It can be observed that NO_x emission distribution for both burners is almost identical with the mean value of 50 ppm, even fluctuations for HSB are slightly higher than those for LSB, but the mean value is slightly lower than that for LSB.

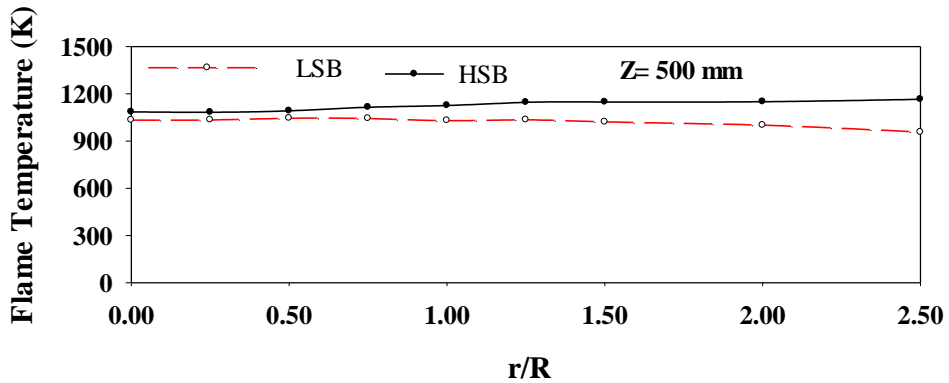


Figure 4-6 Measured radial temperature profile at combustor exit

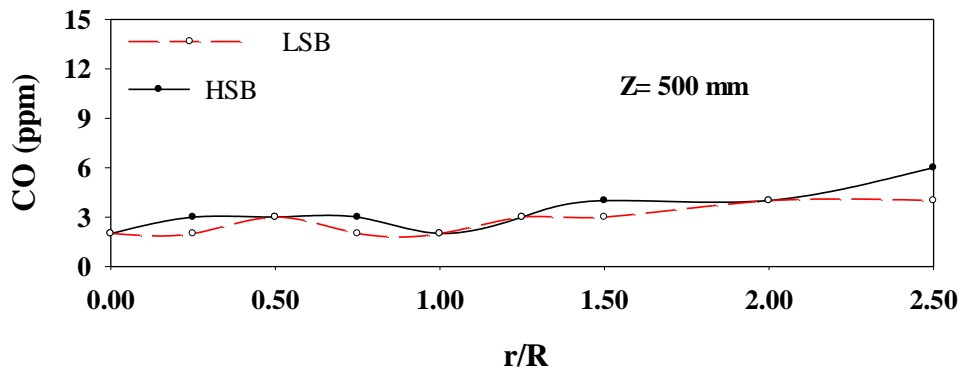


Figure 4-7 Measured radial CO profile at combustor exit

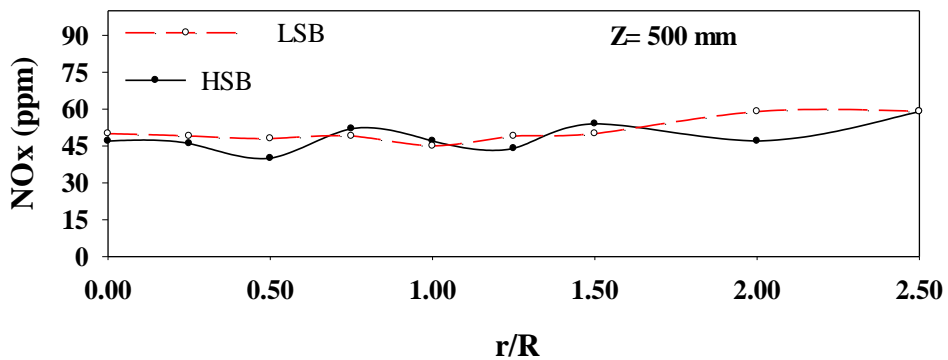


Figure 4-8 Measured radial NO_x profile at combustor exit

Figure 4-9 shows the direct visual images of Jet A-1 LPP swirled flame using both HSB and LSB. As the combustion is lean premixed, both flames appear in blue color, however, due to the region of intensified reaction for HSB in the

recirculation zone, the produced flame has an attached brighter-blue cone-shaped flame stabilized at the burner exit providing a slender flame with a high-temperature zone near the edge of the burner bluff-body. Whereas, the LSB has a lifted lighter-blue (W) type flame which provides much uniform thermal regime in the flame core. These results have a good agreement with those cited in the literature [56].



Figure 4-9 Jet A-1 flame image; HSB (Left) and LSB (Right)

Figure 4-10 shows the radial flame temperature distribution at different axial locations for both HSB and LSB. For LSB at $Z = 10$ mm, the flame temperature in the central area around the burner axis is relatively low and increased to 1525 K at $r/R = 1.5$ due to the existing of lifted flame shape. It should also be noted that, the temperature increases rapidly as Z exceeds 10 mm, and reaches the maximum value in the region of $30 < Z < 50$ mm. Afterward, the temperature decreases slowly until the temperature recalls the uniform profile beyond $Z = 130$ mm. For HSB the highest temperature region (from $Z = 10$ mm to $Z = 70$ mm) occurs in the shear layer where a portion of the hot combustion products is entrained and recirculated to mix with the incoming air-fuel

premixed mixture. Away from the center body edge to the center, the recirculated hot products keep high temperature. On the other side from the center body edge towards the combustor wall, the temperature falls down gradually (as shown in Figure 4-10) in particular at the lower zone of the combustor. Furthermore, with increasing the vertical distance away from the core of the central recirculation zone (beyond $Z = 90$ mm), the flow fluctuation is decayed and the flow becomes more homogeneous, the temperature variation with the radial distance is decreased. Figure 4-11 shows a comparison of the temperature contours. Where zone of high temperature is formed at the burner central axis for LSB, while annulus zone of high temperature around the burner axis is formed for HSB as a result of the existed recirculation zone.

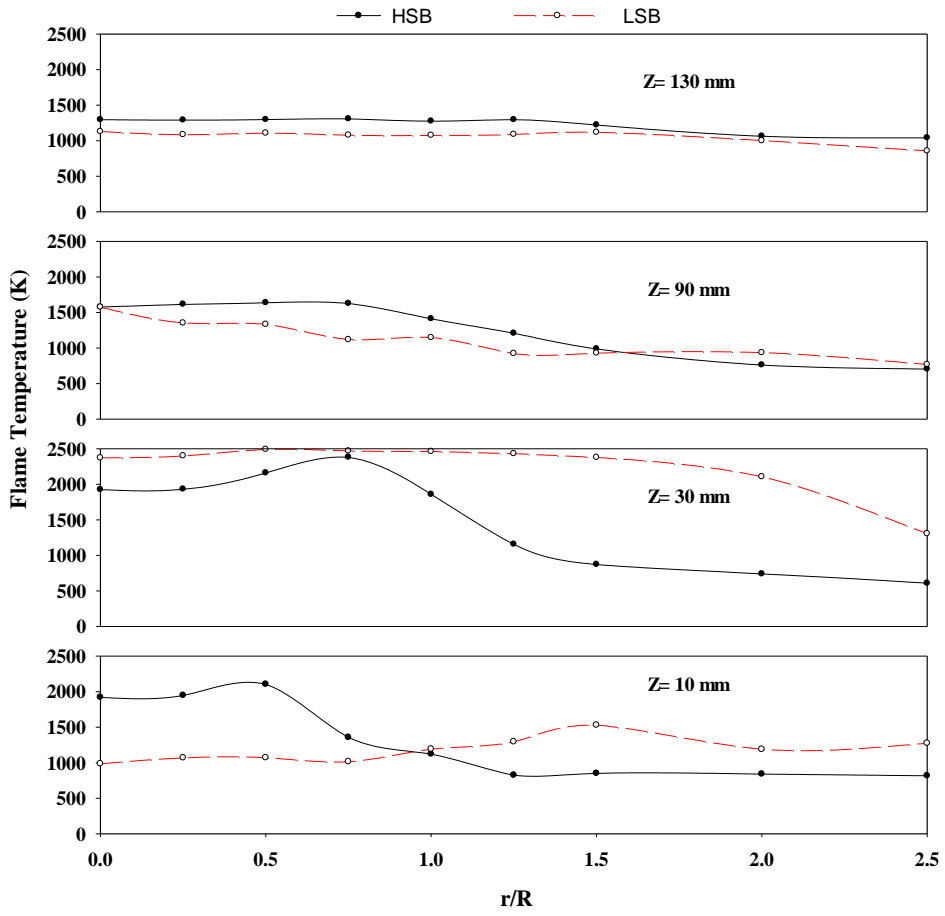
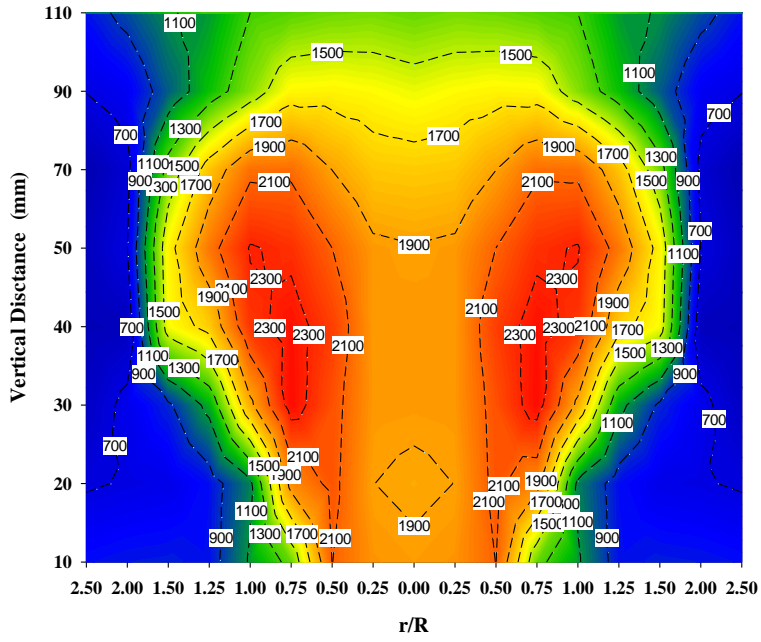
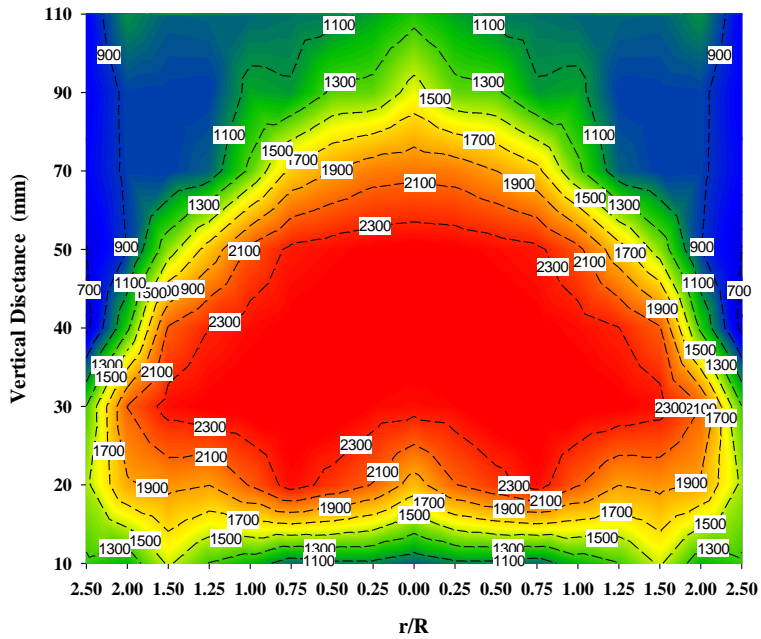


Figure 4-10 Flame temperature radial distribution



(a)



(b)

Figure 4-11 Contours of the flame temperature (K); (a) HSB and (b) LSB

The emissions of LPP swirled combustion is mainly a function of the local flame temperature, turbulence intensity and residence time of flue gas in the high-temperature zone [11]. Figure 4-12 shows that the, CO concentration produced from the Jet A-1 combustion increases rapidly within the range of $20 < Z < 50$ mm, where the local temperature is high and the dissociation reactions of CO_2 to form CO would be significant. The CO concentration decreases with increasing the vertical distance where the mixture homogeneity is improved and the local temperature is reduced; as observed from contours in Figure 4-13. It is also noted that the CO concentrations for LSB decreases as the radial distance from the burner centerline is increased until it reaches the minimum value for the radial plane at the farthest point from the burner centerline. The CO concentration of the HSB has its peak value at the burner edge where the highest flame temperature exists and decreases in the flame core due to the recirculation motion which decreases the flame temperature as moving away from the burner edge to the combustor wall. Overall, the CO values at the combustor exit plane are small (< 6 ppm), compared to CO values of > 23000 ppm within the flame front.

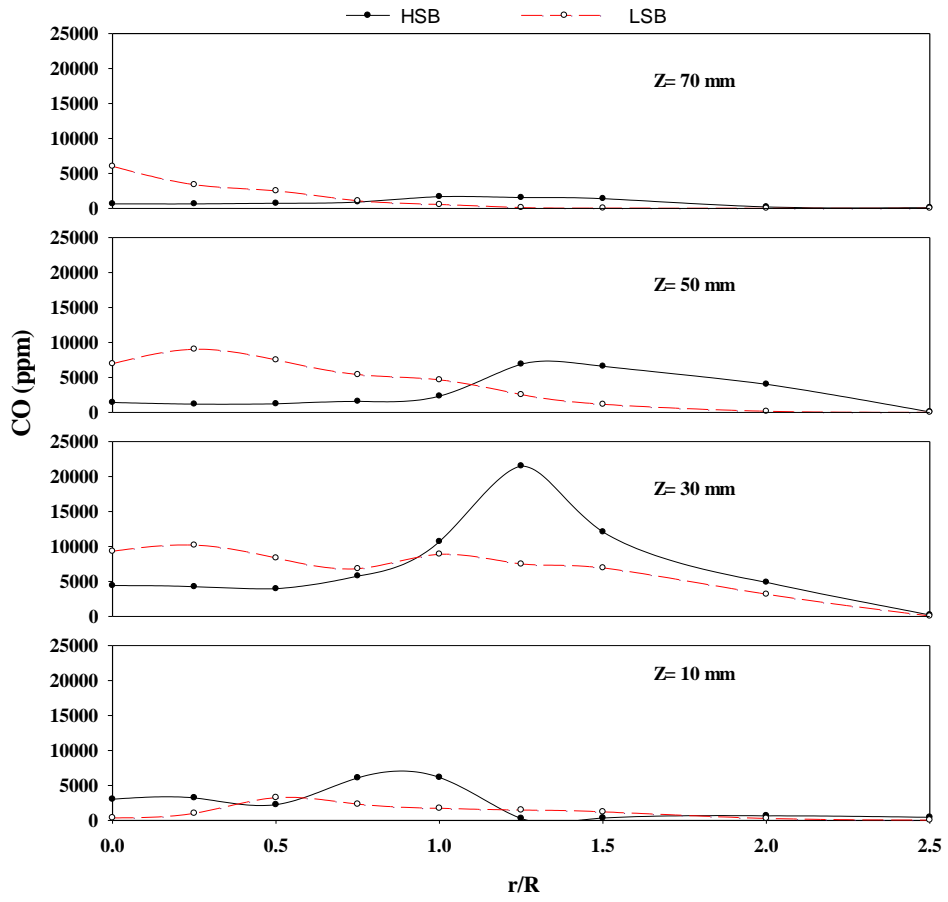


Figure 4-12 In flame CO concentrations radial distribution

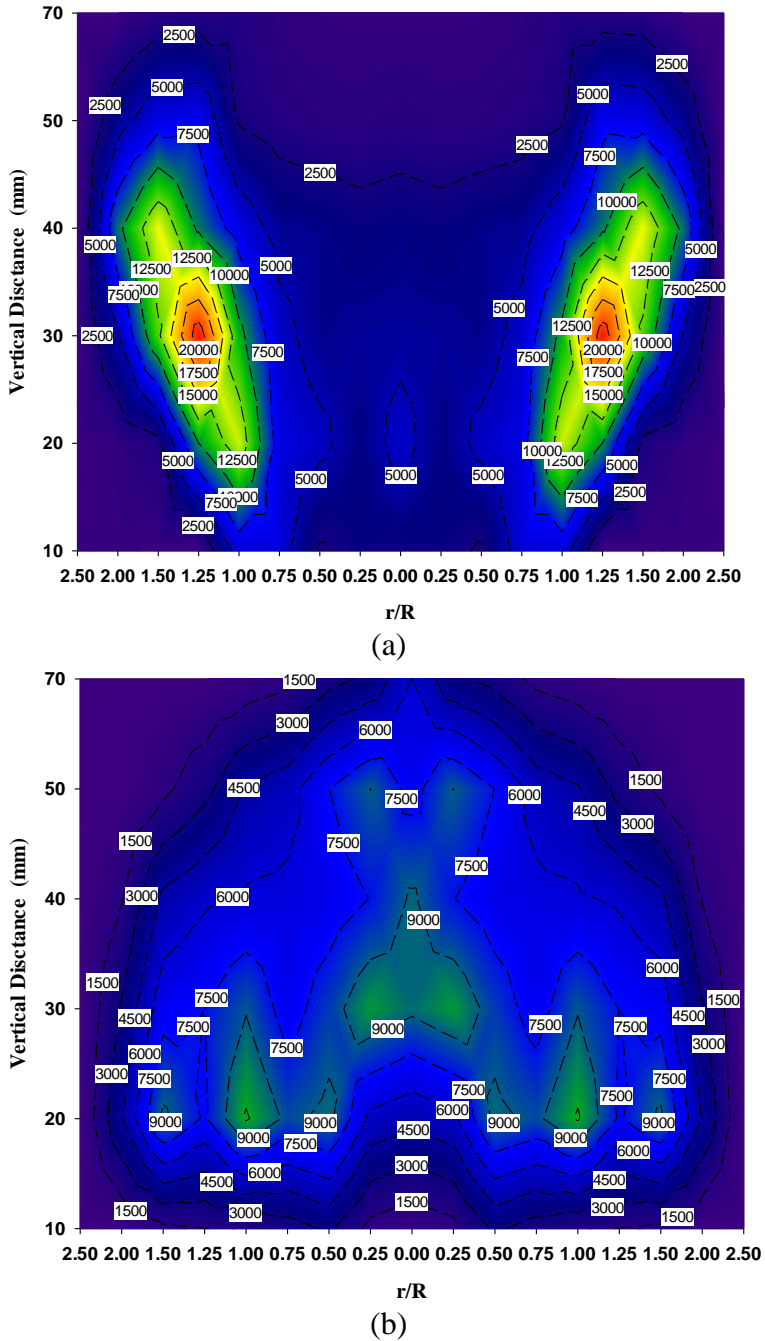


Figure 4-13 Contours of the CO concentrations (ppm); (a) HSB and (b) LSB

The NO_x emissions formed from the premixed combustion is mainly the thermal NO_x . Thermal NO_x mechanism is an endothermic reaction resulting in the creation of NO at high temperatures of about 1850 K [11]. Thermal NO_x formation depends on several factors, such as the local flame temperature, turbulence intensity, residence time of flue gas in the high-temperature zone, and the local equivalence ratio [11]. Figure 4-14 and Figure 4-15 shows a gradual increase in NO_x concentration with increasing the vertical distance towards the combustor exit using LSB until specific level where maximum temperature occurs. The maximum value of the NO_x concentration appears at $Z= 70$ mm in the combustor center. Then the NO_x concentration distribution become more uniform with increasing the vertical distance. Similar behavior is received for HSB, where the maximum value of the NO_x concentration appears at $Z= 70$ mm and $r/R = 1$. However, NO_x concentration of the HSB is higher than that of the LSB because the HSB has a greater residence time within the recirculation zone which provides more time for NO_x formation in addition to the higher temperature in the intensive reaction zone. Near the combustor wall, the NO_x concentration values for HSB are lower than those for LSB because of the heat loss through the combustor wall which produces a cooling effect. These results agreed with those stated in the literature by [20].

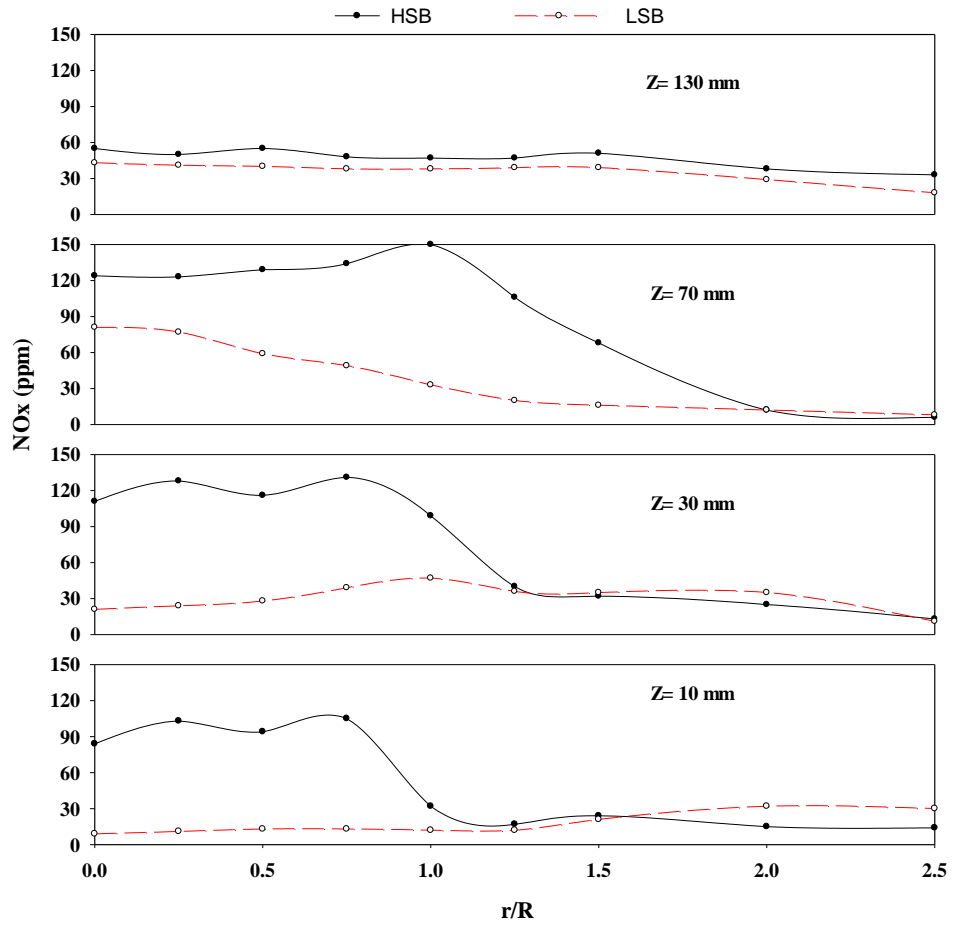
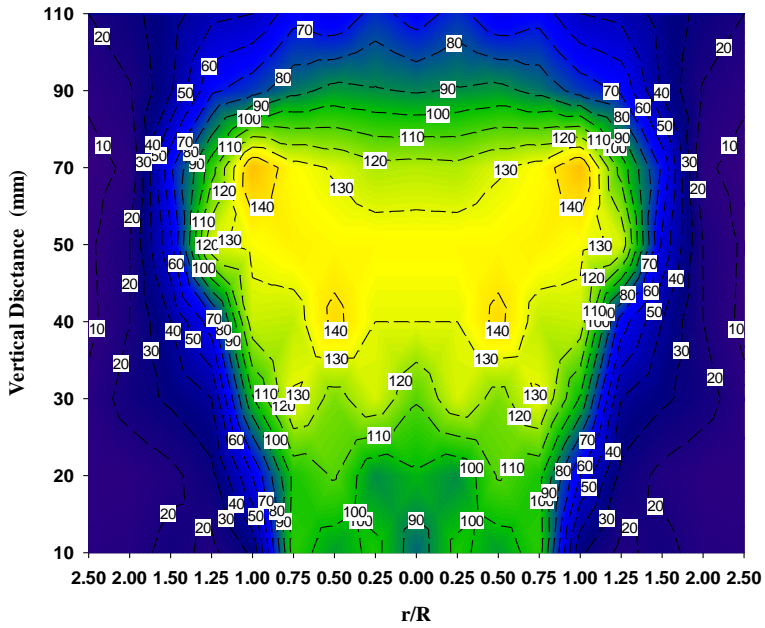
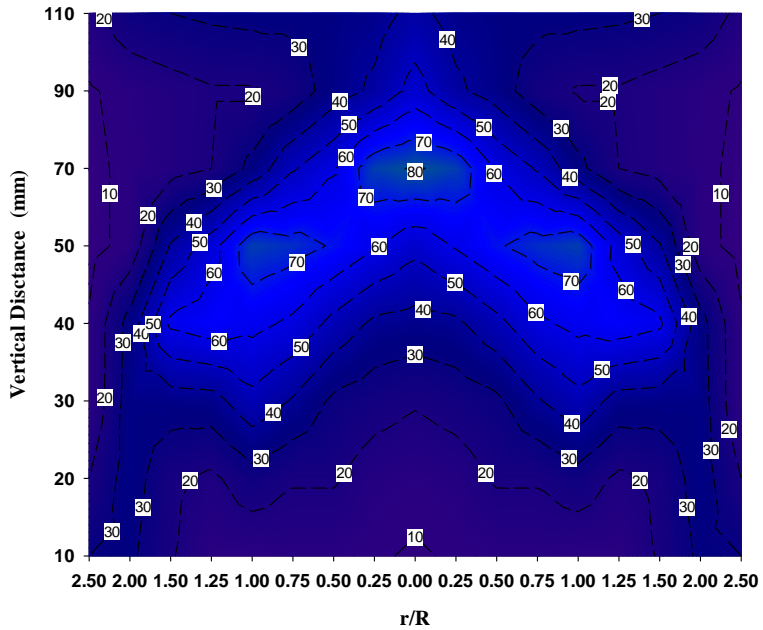


Figure 4-14 In flame NO_x concentrations radial distribution



(a)



(b)

Figure 4-15 Contours of the NO_x concentrations; (a) HSB and (b) LSB

4.4 Effect of Jet A-1/Biodiesel Blends on the Combustion and Emissions Characteristics of HSB

In this section, results about the flame behavior of blended fuels burned in LPP combustion using HSB has been presented. biofuel combustion. The corrected flame temperature distributions at selected vertical planes of blended fuels using different blending ratios for the investigated fuels are shown in Figure 4-16. It is important to notice that, the degree of mixture heterogeneity and so the possibility to get purely premixed or partially premixed combustion of blended fuels depends mainly on the higher boiling point of the biodiesel [57].

In the case of B5 and B10, the flame temperature is slightly higher than that of B0 due to the mixture heterogeneity and combustion of the WCOME as a droplet (partially premixed combustion mode). The biodiesel blending ratio in case of B5 and B10 is small and the mixture viscosity is near the viscosity of B0 which form a small droplets size which in turn evaporated and burned faster than that droplets exist in case of B15 and B20. An additional reason to get higher temperature may be owing to the fact that, the oxygen contents in WCOME accelerates the fuel oxidation with a slight reduction in the blended fuel heating value and so rapid release of energy providing a higher local temperature in the reaction zone. At the higher levels where the biodiesel droplets fade away and the mixture becomes more homogeneous the flame temperature of B10 becomes closer to that of B0.

Ban-Weiss et al. [58] showed that unsaturated molecules exhibit higher adiabatic flame temperature than their saturated counterparts. This has been used to hypothesize that biodiesel gives higher flame temperature than conventional fuels, due to the higher concentration of unsaturated compounds in biodiesel.

The slight reduction in the flame temperature of B20 is mainly due to the effect of the lower heating value of B20 that competes the effect of the higher oxygen contents accelerating the fuel oxidation. The overall results represent that a higher level of similarity between the flame temperature of B0, B5, B10, B15, and B20.

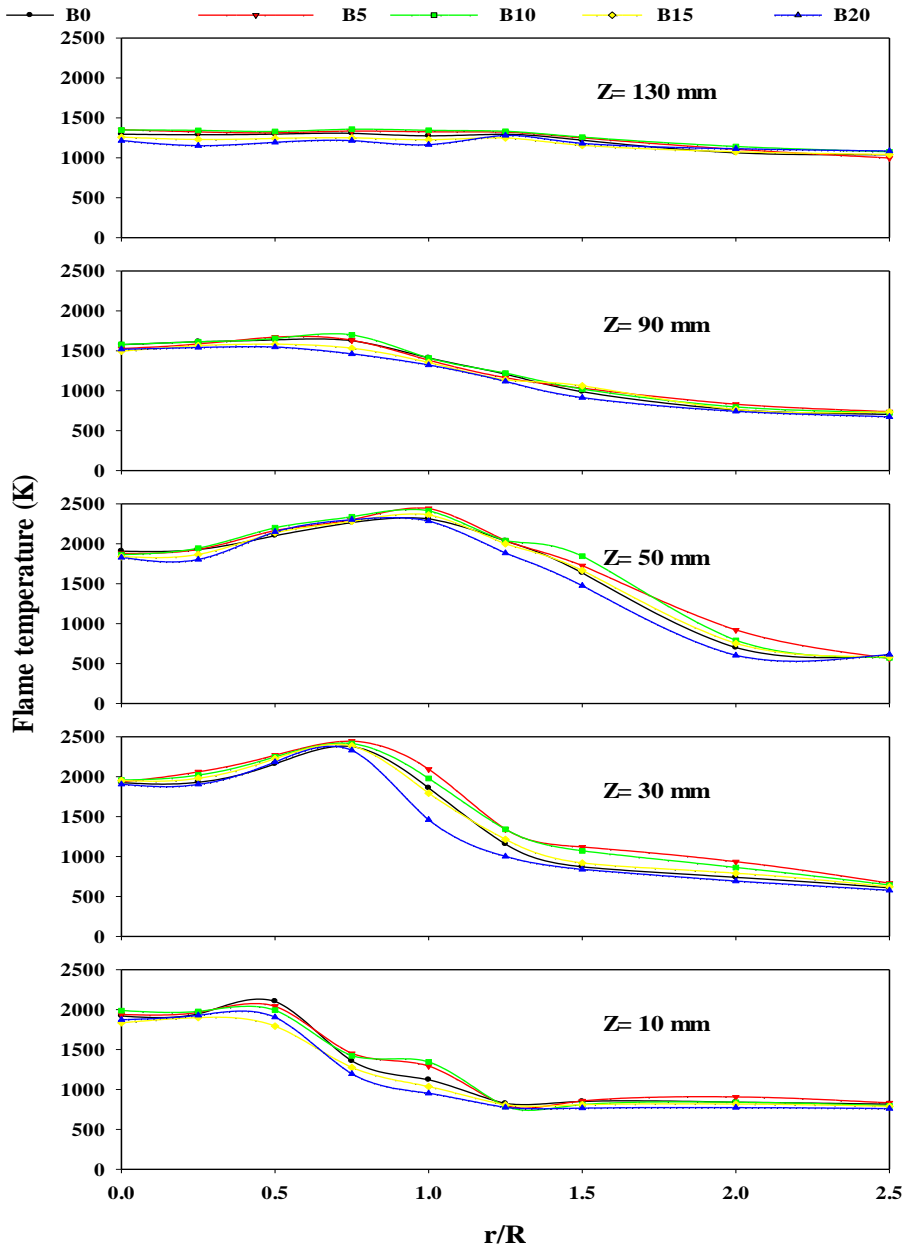


Figure 4-16 In flame temperature radial distribution

The basic factors influencing the formation of emissions (CO and NO_x) in the swirl stabilized LPP combustion are the combustor inlet temperature, the local flame temperature, the combustion pressure, the equivalence ratio, the turbulence intensity, and the residence time of flue gas in the high-temperature zone [11]. With mixing WCOME with Jet A-1 fuel, the blending ratio will be another important factor reflecting the opposing influence of the lower heating value and the oxygen contents of biodiesel. To conduct the effect of blending ratio on the species concentration all other regulated factors are kept constant through the experiments except fuel type; as preheat temperature, and equivalence ratio. Figure 4-17 shows the CO concentrations at selected axial locations throughout the combustor for the investigated fuels.

In the core of Jet A-1 flame where the temperature is relatively low, the CO concentration is decreased as a result of the reduced dissociations of CO₂ into CO at this temperature as reported by [59]. Near the edge of the burner center body, the maximum CO concentrations are achieved as reported by [47] where the dissociation rate of CO₂ is high at a high flame temperature (especially when the temperature exceeds 1900 K). Near the combustor wall, the CO concentration is decreased again to be lower than that in the flame core. As the vertical distance is increased, the mixture becomes more homogeneous and the CO concentration decreases to reach the minimum value at the combustor exit. By the comparison, the CO concentration of all the tested fuels has a comparable value with that of Jet A-1 at the lower levels in the combustor ($Z=10$ mm) and it is started to increase at high vertical distance reaching its maximum deviation at $Z=30$ mm. The peak of CO concentration for Jet A-1 is approximately twice that for B20 and this gap was getting smaller with increasing the vertical distance. This reduction of CO concentration for B20 is mainly due to the oxygen content in biodiesel which promotes fuel oxidation

and so complete combustion [60].

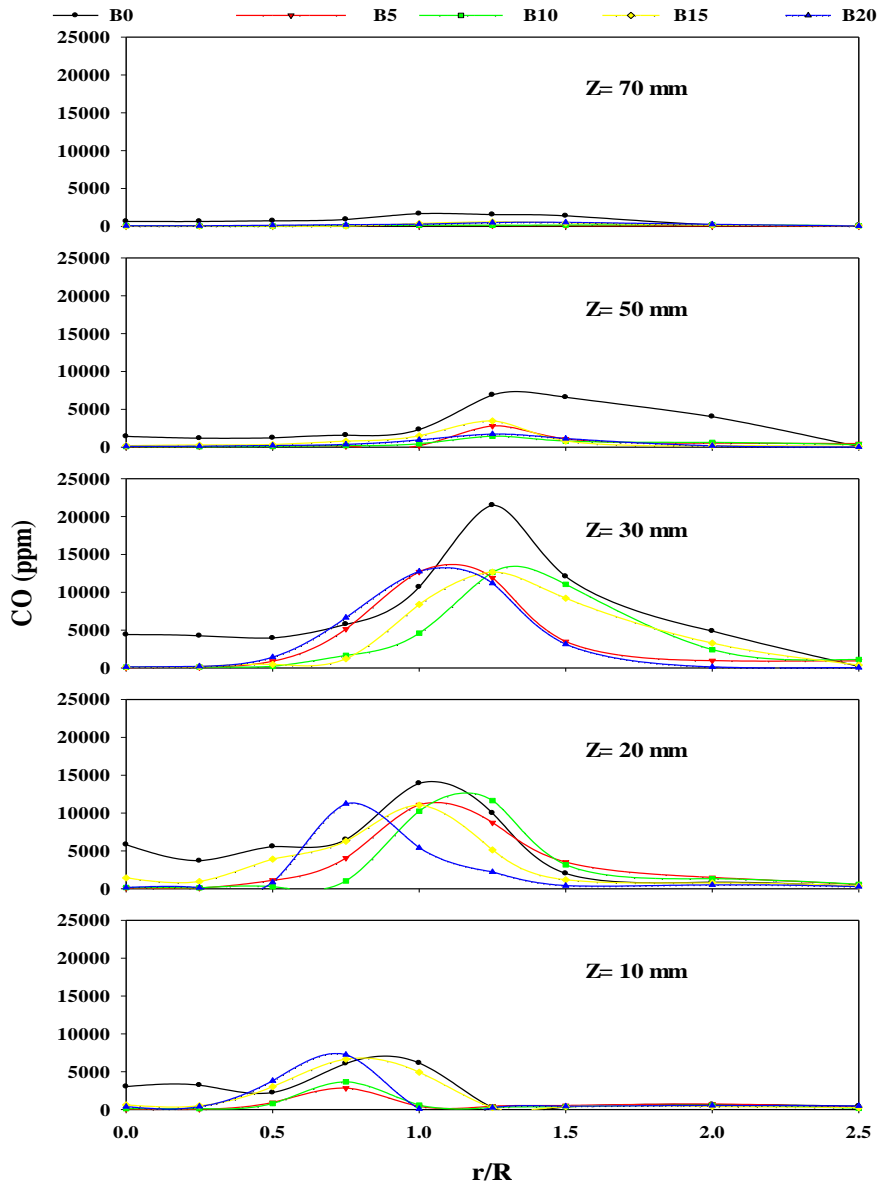
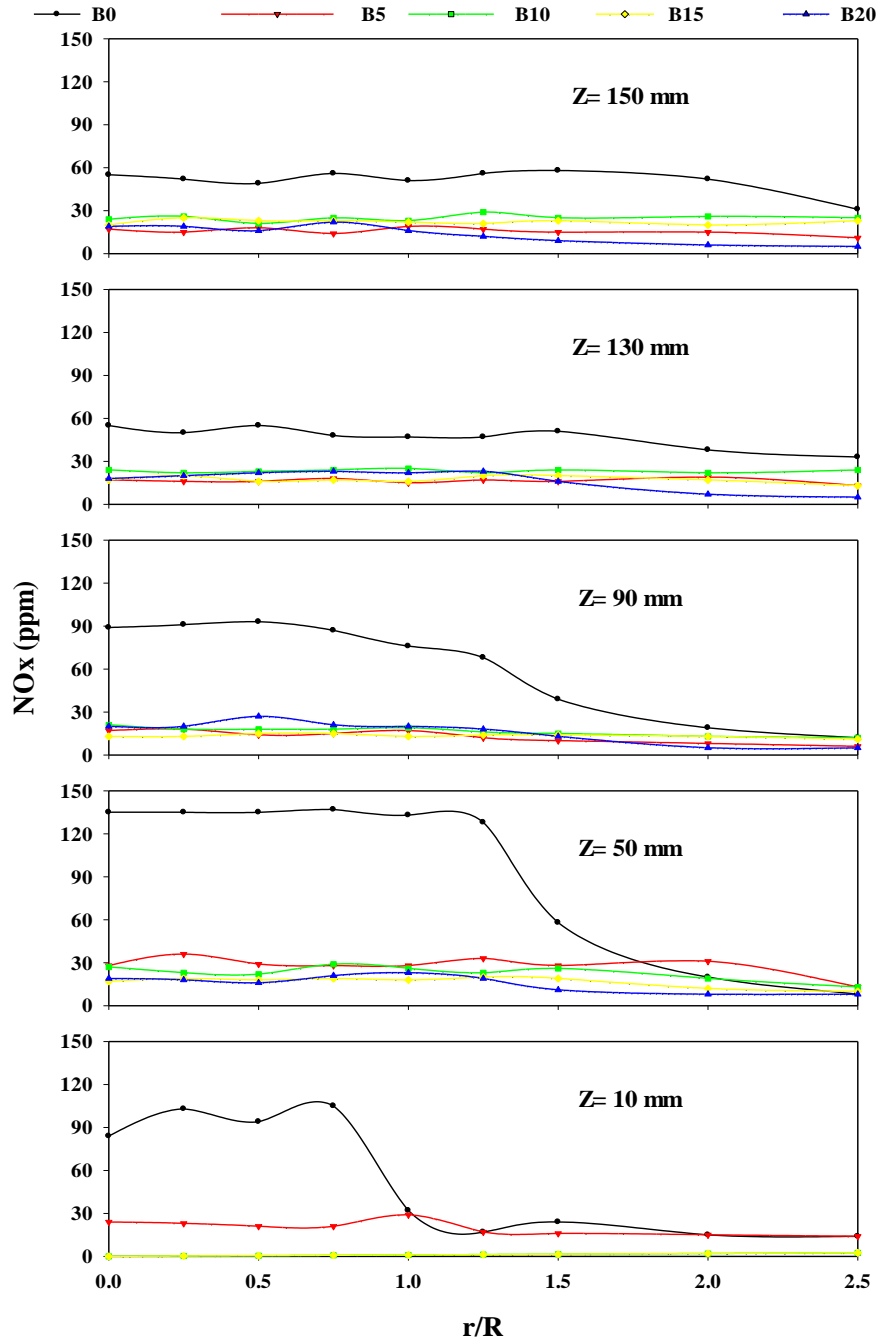


Figure 4-17 In flame CO concentrations radial distribution

The NO_x concentrations of the LPP swirl stabilized combustion at selected axial locations throughout the combustor including Jet A-1 fuel and its blends are shown in Figure 4-18. The NO_x concentrations of Jet A-1 increase with increasing the vertical distance towards the combustor exit. The maximum NO_x concentration appears after getting the maximum temperature at $Z = 50$ mm then NO_x concentrations are decreased rapidly with increasing the vertical distance towards the combustor exit as a result of temperature decrease. The NO_x concentrations for biodiesel blends are remarkably lower than those for Jet A-1 even there is a slight temperature difference as confirmed by [47]. The reduction of NO_x emitted from biodiesel blends combustion can be related to biodiesel properties as biodiesel is comprised of shorter hydrocarbon chains result in a lower flame temperature and thus decrease the thermal NO_x formation [60]. Also, the high oxygen content existed in the WCOME enhances the combustion process also increase the formation of some active radicals such as OH [11]. This plays a significant role in Zeldovich mechanism of thermal NO_x formation and may be one of the major reasons for this different NO_x concentration behavior. The accurate reason for NO_x reduction of biodiesel is not yet clear as there is no complete chemical reaction mechanism for biodiesel combustion available till now [58].

Figure 4-18 In flame NO_x concentrations radial distribution

4.5 Effect of Jet A-1/Biodiesel Blends on the Combustor Thermal Uniformity

The thermal uniformity through the combustor represented by pattern factor (PF) is one of the major parameters that shall be considered in gas turbine combustion [11]. Lower values of the PF reflect a more thermal uniformity and excessively high values can be indicative of dangers to turbine components due to localized hot spots. As shown in Figure 4-19 for Jet A-1 the PF decreases with increasing the vertical distance and so thermal uniformity of the combustor is increased. For the B20 the PF value decreases with increasing the vertical distance. This different behavior is due to the WCOME droplets combustion existed at the lower zone in the combustor. At the higher zone in the combustor ($Z > 150$ mm) the PF of the B20 is lower than that of the Jet A-1. B5, B10, and B15 enhanced the thermal uniformity of the combustor, especially at lower levels.

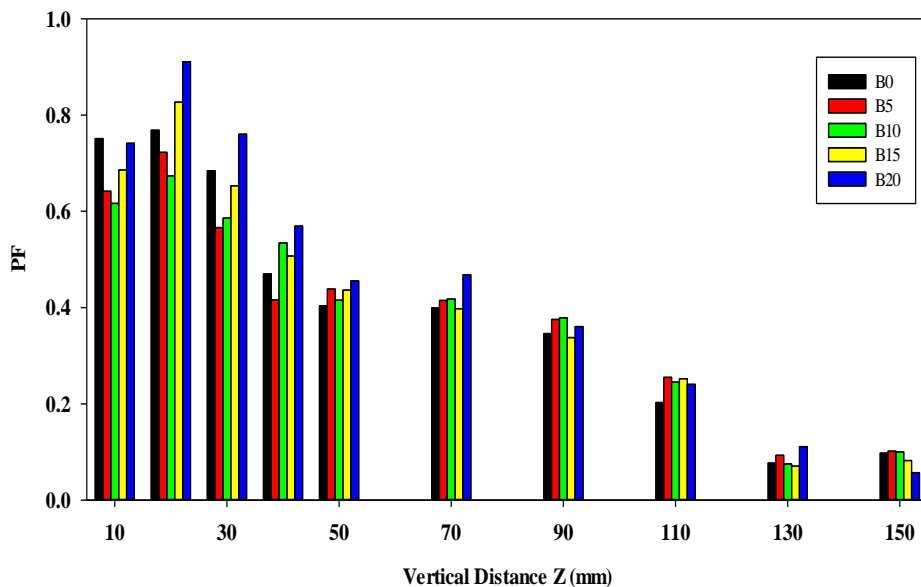


Figure 4-19 Combustor pattern factor for tested fuels

4.6 Environmental Impact of The Waste Cooking Oil Biodiesel

The NO emission index (EI_{NO_x}) and CO emission indices (EI_{CO}) obtained from the combustion of the tested fuels are shown in Figure 4-20 and Figure 4-21. The results demonstrated that Jet A-1 produces the highest NO_x emission index, followed by B10, B15, 20 and B5, resulting in a 31% reduction for B10, 34% reduction for B15, 41% reduction for B20 and a 45% reduction for B5. B10 produces the highest CO emission index due to the increase in the local flame temperature while B20 produces the lowest CO emission index due to the high oxygen content of biodiesel and produces 30% lower CO than Jet A-1. The CO emission index for B5 and B10 are higher than those of Jet A-1 due to the increase in the local flame temperature.

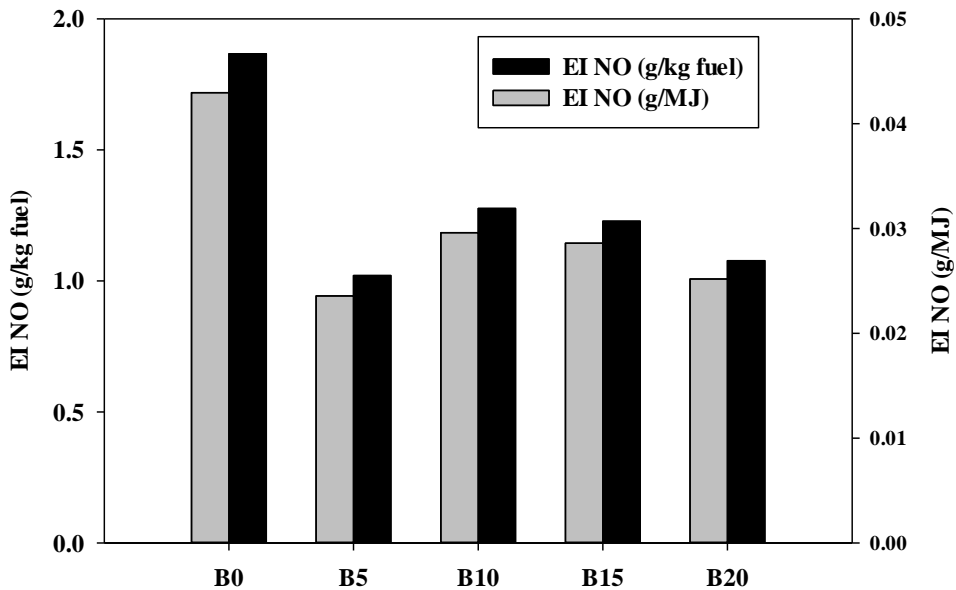


Figure 4-20 Emission index of nitrogen oxides

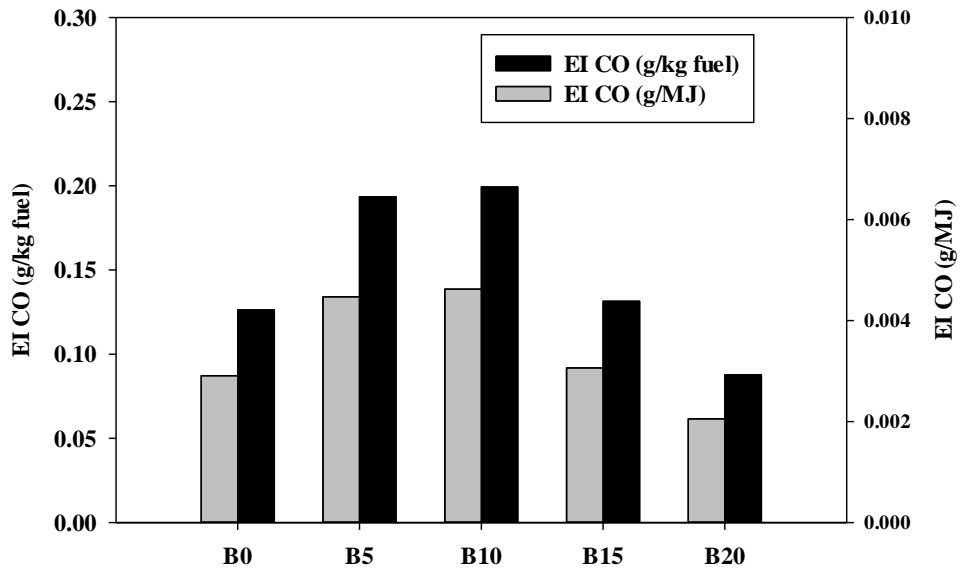


Figure 4-21 Emission index of carbon monoxide

Chapter 5: CONCLUSIONS

The current study aimed to investigate the flame characteristics of biodiesel / Jet A-1 blends burned in Lean Pre-vaporized Premixed (LPP) combustor. To stabilize these flames, different burner designs having the same swirl numbers were constructed. The biodiesel was produced from waste cooking oil with the help of ultrasonic. The experiments include cold flow as well as flame measurements through LPP combustor. In the later, set of experiments were performed at constant conditions of preheated temperature and equivalence ratio, while regulating the blending ratio as well as the burner type. Initially, Jet A-1 flame structures were determined using two different burners (high swirl and low swirl burners abbreviated as HSB and LSB; respectively), then HSB was used to investigate the effect of blending ratio of biodiesel on flame structure of blended fuels (containing 5, 10, 15, and 20% biodiesel mixed with Jet A-1 as base fuel). The main conclusion from this work is that the lean combustion of premixed mixtures from air with blended fuels not only can improve the emission parameters but also can improve the thermal characteristics of combustor up to a blending ratio of 20%. From the whole results related to biodiesel production, cold flow, and combustion characteristics, the following specific conclusions can be drawn:

1. Use of ultrasonic in biodiesel production remarkably reduces the production period from almost 1.5 hr. to 0.25 hr.
2. The flow field of the LSB is free of a central recirculation zone while HSB has a large central recirculation region.;
3. The HSB can generate an attached blue cone-shaped flame while the LSB can generate a blue lift-off “W” type flame.

4. The HSB flame temperature distribution shows a high-temperature zone on the burner edge which represent a hot spot region. While the LSB shows a more uniform flame temperature distribution.
5. The CO and NO_x concentrations of the HSB through the flame are approximately 50 % higher than LSB due to the recirculation and long residence time of combustion product in hot reaction zone.
6. The CO and NO_x concentrations at the combustor exit plane are comparable.
7. The local flame temperature distribution of blended fuels was comparable to that of Jet A-1, except for B20 it was slightly lower than that of Jet A-1.
8. There was a remarkable reduction of the exhaust emissions due to biodiesel blending, the maximum reduction in CO was received for B20 (30%) and the maximum reduction for NO_x was received at B5 (45%).
9. The CO emission index for B5 and B10 at the combustor exit were increased by 54% and 59% respectively compared to pure Jet A-1 fuel due to the increase in the local flame temperature.
10. The NO_x emission index of B20 at the combustor exit was decreased significantly by 41% compared to pure Jet A-1 fuel.
11. The Jet A-1 fuel can be replaced by B20 without any modifications in the combustor design as they have similar temperature distribution and significant emission reduction.

REFERENCE

- [1] Kumar, R. S., Sureshkumar, K., & Velraj, R. (2015). Optimization of biodiesel production from Manilkara zapota (L.) seed oil using Taguchi method. *Fuel*, 140, 90-96.
- [2] Sakthivel, R., Ramesh, K., Purnachandran, R., & Shameer, P. M. (2018). A review on the properties, performance and emission aspects of the third generation biodiesels. *Renewable and Sustainable Energy Reviews*, 82, 2970-2992.
- [3] Mazanov, S. V., Gabitova, A. R., Usmanov, R. A., Gumerov, F. M., Labidi, S., Amar, M. B., & Le Neindre, B. (2016). Continuous production of biodiesel from rapeseed oil by ultrasonic assist transesterification in supercritical ethanol. *The Journal of Supercritical Fluids*, 118, 107-118.
- [4] Awadallak, J. A., Voll, F., Ribas, M. C., da Silva, C., Cardozo Filho, L., & da Silva, E. A. (2013). Enzymatic catalyzed palm oil hydrolysis under ultrasound irradiation: diacylglycerol synthesis. *Ultrasonics sonochemistry*, 20(4), 1002-1007.
- [5] Aboelazayem, O., El-Gendy, N., Abdel-Rehim, A. A., Ashour, F., & Sadek, M. A. (2018). Biodiesel production from castor oil in Egypt: process optimisation, kinetic study, diesel engine performance and exhaust emissions analysis. *Energy*.
- [6] Torres-Rodríguez, D. A., Romero-Ibarra, I. C., Ibarra, I. A., & Pfeiffer, H. (2016). Biodiesel production from soybean and *Jatropha* oils using

cesium impregnated sodium zirconate as a heterogeneous base catalyst. *Renewable Energy*, 93, 323-331.

- [7] Sandouqa, A., & Al-Hamamre, Z. (2019). Energy analysis of biodiesel production from jojoba seed oil. *Renewable energy*, 130, 831-842.
- [8] Supardan, M., Satriana, S., & Mahlinda, M. (2013). Biodiesel Production from Waste Cooking Oil Using Hydrodynamic Cavitation. *Makara Journal of Technology*, 16(2), 157-162.
- [9] Kirubakaran, M., & Selvan, V. A. M. (2018). A comprehensive review of low cost biodiesel production from waste chicken fat. *Renewable and Sustainable Energy reviews*, 82, 390-401.
- [10] Kara, K., Ouanji, F., Lotfi, E. M., El Mahi, M., Kacimi, M., & Ziyad, M. (2018). Biodiesel production from waste fish oil with high free fatty acid content from Moroccan fish-processing industries. *Egyptian Journal of Petroleum*, 27(2), 249-255.
- [11] Lefebvre, A. H., & Ballal, D. R. (2010). *Gas turbine combustion: alternative fuels and emissions*. CRC press.
- [12] Turns, S. R. (2000). *An introduction to combustion*, 2000. MacGraw Hill, Boston, Massachusetts, US.
- [13] Al-Abdeli, Y. M., & Masri, A. R. (2015). Review of laboratory swirl burners and experiments for model validation. *Experimental Thermal and Fluid Science*, 69, 178-196.
- [14] Beér, J. M., & Chigier, N. A. (1972). *Combustion aerodynamics*. New York.

- [15] Chterev, I., Foley, C. W., Foti, D., Kostka, S., Caswell, A. W., Jiang, N., & Lieuwen, T. C. (2014). Flame and flow topologies in an annular swirling flow. *Combustion Science and Technology*, 186(8), 1041-1074.
- [16] Therkelsen, P. L., Littlejohn, D., & Cheng, R. K. (2012). Parametric study of low-swirl injector geometry on its operability. In *ASME Turbo Expo 2012: Turbine Technical Conference and Exposition* (pp. 309-318). American Society of Mechanical Engineers.
- [17] Cheng, R. K., Yegian, D. T., Miyasato, M. M., Samuelsen, G. S., Benson, C. E., Pellizzari, R., & Loftus, P. (2000). Scaling and development of low-swirl burners for low-emission furnaces and boilers. *Proceedings of the Combustion Institute*, 28(1), 1305-1313.
- [18] Colorado, A. (2016). Pollutant Emissions and Lean Blowoff Limits of Fuel Flexible Burners Operating on Gaseous Renewable and Fossil Fuels. Doctoral dissertation, UC Irvine.
- [19] Therkelsen P. (2016). *Advancements in Atmospheric Combustion*. American Society of Gas Engineers.
- [20] Johnson, M. R., Littlejohn, D., Nazeer, W. A., Smith, K. O., & Cheng, R. K. (2005). A comparison of the flowfields and emissions of high-swirl injectors and low-swirl injectors for lean premixed gas turbines. *Proceedings of the Combustion Institute*, 30(2), 2867-2874.
- [21] Littlejohn, D., & Cheng, R. K. (2007). Fuel effects on a low-swirl injector for lean premixed gas turbines. *Proceedings of the Combustion Institute*, 31(2), 3155-3162.

- [22] Legrand, M., Nogueira, J., Lecuona, A., Nauri, S., & Rodríguez, P. A. (2010). Atmospheric low swirl burner flow characterization with stereo PIV. *Experiments in fluids*, 48(5), 901-913.
- [23] Cheng, R. K., & Littlejohn, D. (2008). Effects of combustor geometry on the flowfields and flame properties of a low-swirl injector. In *ASME Turbo Expo 2008: Power for Land, Sea, and Air* (pp. 393-407). American Society of Mechanical Engineers.
- [24] Littlejohn, D., Majeski, A. J., Tonse, S., Castaldini, C., & Cheng, R. K. (2002). Laboratory investigation of an ultralow NO_x premixed combustion concept for industrial boilers. *Proceedings of the combustion institute*, 29(1), 1115-1121.
- [25] Cheng, R. K., Littlejohn, D., Strakey, P. A., & Sidwell, T. (2009). Laboratory investigations of a low-swirl injector with H₂ and CH₄ at gas turbine conditions. *Proceedings of the Combustion Institute*, 32(2), 3001-3009.
- [26] Day, M., Tachibana, S., Bell, J., Lijewski, M., Beckner, V., & Cheng, R. K. (2012). A combined computational and experimental characterization of lean premixed turbulent low swirl laboratory flames: I. Methane flames. *Combustion and Flame*, 159(1), 275-290.
- [27] Feyz, M. E., Esfahani, J. A., Pishbin, I., & Razavi, S. M. (2015). Effect of recess length on the flame parameters and combustion performance of a low swirl burner. *Applied Thermal Engineering*, 89, 609-617.

- [28] Koyama, M., & Tachibana, S. (2013). Technical applicability of low-swirl fuel nozzle for liquid-fueled industrial gas turbine combustor. *Fuel*, 107, 766-776.
- [29] Sequera, D., & Agrawal, A. K. (2007). Effect of Fuel Composition on Emissions From a Low-Swirl Burner. In *ASME Turbo Expo 2007: Power for Land, Sea, and Air* (pp. 789-799). American Society of Mechanical Engineers.
- [30] Bruton, D. J. (2014). Waste Cooking Oil-to-Biodiesel Conversion for Space Heating Applications. M.Sc. Thesis, Rochester Institute of Technology.
- [31] Karmakar, A., Karmakar, S., & Mukherjee, S. (2010). Properties of various plants and animals feedstocks for biodiesel production. *Bioresource technology*, 101(19), 7201-7210.
- [32] Meher, L. C., Sagar, D. V., & Naik, S. N. (2006). Technical aspects of biodiesel production by transesterification—a review. *Renewable and sustainable energy reviews*, 10(3), 248-268.
- [33] Attia, A. M., & Hassaneen, A. E. (2016). Influence of diesel fuel blended with biodiesel produced from waste cooking oil on diesel engine performance. *Fuel*, 167, 316-328.
- [34] Refaat, A. A., Attia, N. K., Sibak, H. A., El Sheltawy, S. T., & ElDiwani, G. I. (2008). Production optimization and quality assessment of biodiesel from waste vegetable oil. *International Journal of Environmental Science & Technology*, 5(1), 75-82.

- [35] Ibrahim, M. N., Ali, A. H. H., & Ookawara, S. (2013). Performance assessment of turbojet engine operated with alternative biodiesel. In ASME 2013 Power Conference. American Society of Mechanical Engineers.
- [36] Ho, W. W. S., Ng, H. K., & Gan, S. (2016). Advances in ultrasound-assisted transesterification for biodiesel production. *Applied thermal engineering*, 100, 553-563.
- [37] Yu, D., Tian, L., Wu, H., Wang, S., Wang, Y., Ma, D., & Fang, X. (2010). Ultrasonic irradiation with vibration for biodiesel production from soybean oil by Novozym 435. *Process Biochemistry*, 45(4), 519-525.
- [38] Kumar, D., Kumar, G., & Singh, C. P. (2010). Ultrasonic-assisted transesterification of *Jatropha curcus* oil using solid catalyst, Na/SiO₂. *Ultrasonics Sonochemistry*, 17(5), 839-844.
- [39] Samani, B. H., Zareiforoush, H., Lorigooini, Z., Ghobadian, B., Rostami, S., & Fayyazi, E. (2016). Ultrasonic-assisted production of biodiesel from *Pistacia atlantica* Desf. oil. *Fuel*, 168, 22-26.
- [40] El-Mahallawy, F., & Habik, S. D. (2002). *Fundamentals and technology of combustion*. Elsevier.
- [41] Fenimore, C. P. (1971, January). Formation of nitric oxide in premixed hydrocarbon flames. In *Symposium (International) on Combustion (Vol. 13, No. 1, pp. 373-380)*. Elsevier.
- [42] Temme, J. E., Allison, P. M., & Driscoll, J. F. (2014). Combustion instability of a lean premixed prevaporized gas turbine combustor studied using phase-averaged PIV. *Combustion and Flame*, 161(4), 958-970.

- [43] Dhanuka, S. K., Temme, J. E., & Driscoll, J. F. (2011). Lean-limit combustion instabilities of a lean premixed prevaporized gas turbine combustor. *Proceedings of the Combustion Institute*, 33(2), 2961-2966.
- [44] Imamura, A., Yoshida, M., Kawano, M., Aruga, N., Nagata, Y., & Kawagishi, M. (2001). Research and development of a LPP combustor with swirling flow for low NO (x). In *37th Joint Propulsion Conference and Exhibit* (p. 3311).
- [45] Yan, Y., Dang, L., Deng, Y., Li, J., & Zhao, J. (2015). Experimental study of flow dynamics and fuel spray characteristics in Lean Premixed Prevaporized Combustor. *Fuel*, 144, 197-204.
- [46] Gokulakrishnan, P., Ramotowski, M. J., Gaines, G., Fuller, C., Joklik, R., Eskin, L. D., ... & Roby, R. J. (2008). A novel low nox lean, premixed, and prevaporized combustion system for liquid fuels. *Journal of engineering for gas turbines and power*, 130(5).
- [47] Attia, A. M., El-Zoheiry, R. M., El-Batsh, H. M., & Shehata, M. S. (2014, November). Combustion Characteristics of Jojoba Methyl Ester as an Alternative Fuel for Gas Turbine. In *ASME 2014 International Mechanical Engineering Congress and Exposition*. American Society of Mechanical Engineers.
- [48] Hashimoto, N., Ozawa, Y., Mori, N., Yuri, I., & Hisamatsu, T. (2008). Fundamental combustion characteristics of palm methyl ester (PME) as alternative fuel for gas turbines. *Fuel*, 87(15-16), 3373-3378.

- [49] Hashimoto, N., Nishida, H., & Ozawa, Y. (2014). Fundamental combustion characteristics of Jatropha oil as alternative fuel for gas turbines. *Fuel*, 126, 194-201.
- [50] Habib, Z., Parthasarathy, R., & Gollahalli, S. (2010). Performance and emission characteristics of biofuel in a small-scale gas turbine engine. *Applied Energy*, 87(5), 1701-1709.
- [51] El-Zoheiry, R. M. (2014). Investigation of Combustion Characteristics for Prevaporized Premixed Biofuel-Jet Mixtures. M.Sc. Thesis, Benha University.
- [52] Dent Jr, T. J. (2012). Mesoscale power generation incorporating heat-recirculation, porous inert media, and thermoelectric modules. Doctoral dissertation, The University of Alabama.
- [53] Cengel, Y. A. (1997). Introduction to thermodynamics and heat transfer. New York: McGraw-Hill.
- [54] Poling, B. E., Prausnitz, J. M., & O'connell, J. P. (2001). The properties of gases and liquids (Vol. 5). New York: Mcgraw-hill.
- [55] Johnson, M. R., & Cheng, R. K. (2003). Dynamics of the flame flowfields in a low-swirl burner. Lawrence Berkeley National Lab, Berkeley, CA (United States).
- [56] Verbeek, A. A., Bouten, T. W., Stoffels, G. G., Geurts, B. J., & van der Meer, T. H. (2015). Fractal turbulence enhancing low-swirl combustion. *Combustion and Flame*, 162(1), 129-143.

- [57] Erazo Jr, J. A., Parthasarathy, R., & Gollahalli, S. (2010). Atomization and combustion of canola methyl ester biofuel spray. *Fuel*, 89(12), 3735-3741.
- [58] Ban-Weiss, G. A., Chen, J. Y., Buchholz, B. A., & Dibble, R. W. (2007). A numerical investigation into the anomalous slight NO_x increase when burning biodiesel; a new (old) theory. *Fuel processing technology*, 88(7), 659-667.
- [59] Shehata, M. (2009). Emissions and wall temperatures for lean prevaporized premixed gas turbine combustor. *Fuel*, 88(3), 446-455.
- [60] Abdul Malik, M. S., Shaiful, A. I. M., Mohd Ismail, M. S., Mohd Jaafar, M. N., & Mohamad Sahar, A. (2017). Combustion and Emission Characteristics of Coconut-Based Biodiesel in a Liquid Fuel Burner. *Energies*, 10(4), 458.

Appendix A THERMOCOUPLES CALIBRATION

The combustor wall temperature is measured using 12 thermocouples type K in conjunction with the data acquisition system described in Appendix B. A standard mercury thermometer of range (0-110 °C) with an accuracy of 1 °C is used to calibrate these thermocouples. The calibration process is conducted using oil heated in glass beaker by means of an electrical heater. During the calibration process, a one thousand reading is acquired by the data acquisition system and the average value of them is calculated and considered as the thermocouple reading.

Table A- 1 Wall thermocouple coordination and calibration equation

Points	Point coordination		Calibration equation
	R (mm)	Z (mm)	
1-	75	30	$T_{ac} (^{\circ}C) = 0.9668 \times DAQ + 2.5653$
2-	75	50	$T_{ac} (^{\circ}C) = 0.9927 \times DAQ + 1.6281$
3-	75	70	$T_{ac} (^{\circ}C) = 0.9546 \times DAQ + 3.4347$
4-	75	110	$T_{ac} (^{\circ}C) = 0.9511 \times DAQ + 2.9273$
5-	75	150	$T_{ac} (^{\circ}C) = 0.9975 \times DAQ + 1.4716$
6-	75	190	$T_{ac} (^{\circ}C) = 0.9821 \times DAQ + 1.9575$
7-	75	230	$T_{ac} (^{\circ}C) = 0.9606 \times DAQ + 2.8461$
8-	75	270	$T_{ac} (^{\circ}C) = 0.9687 \times DAQ + 2.4875$
9-	75	310	$T_{ac} (^{\circ}C) = 0.9768 \times DAQ + 2.2395$
10-	75	350	$T_{ac} (^{\circ}C) = 0.9573 \times DAQ + 2.6487$
11-	75	410	$T_{ac} (^{\circ}C) = 0.98 \times DAQ + 2.4056$
12-	75	470	$T_{ac} (^{\circ}C) = 0.9799 \times DAQ + 2.1506$

Appendix B DATA ACQUISITION SYSTEM

Data acquisition is the process of sampling signals that measure real world physical conditions and converting the resulting samples into digital numeric values that can be manipulated by a computer. Data acquisition systems (abbreviated with the acronym DAQ) typically convert analog waveforms into digital values for processing. The components of data acquisition systems include:

1. Sensors that convert physical parameters to electrical signals.
2. Signal conditioning circuitry to convert sensor signals into a form that can be converted to digital values.
3. Analog-to-digital converters, which convert conditioned sensor signals to digital values.

Simply the DAQ system used in this study is consists of the following items:

4. The NI cDAQ-9178 (eight slots) USB chassis shown in Figure B- 1. The NI cDAQ-9178 chassis can measure a broad range of analog and digital I/O signals and sensors using a Hi-Speed USB 2.0 interface.
5. NI 9213 16-Channel Thermocouple Input Module shown in Figure B- 3. The NI 9213 has a 36-terminal detachable spring-terminal connector that provides connections for 16 thermocouple channels. The terminal assignments are shown in Figure B- 3.

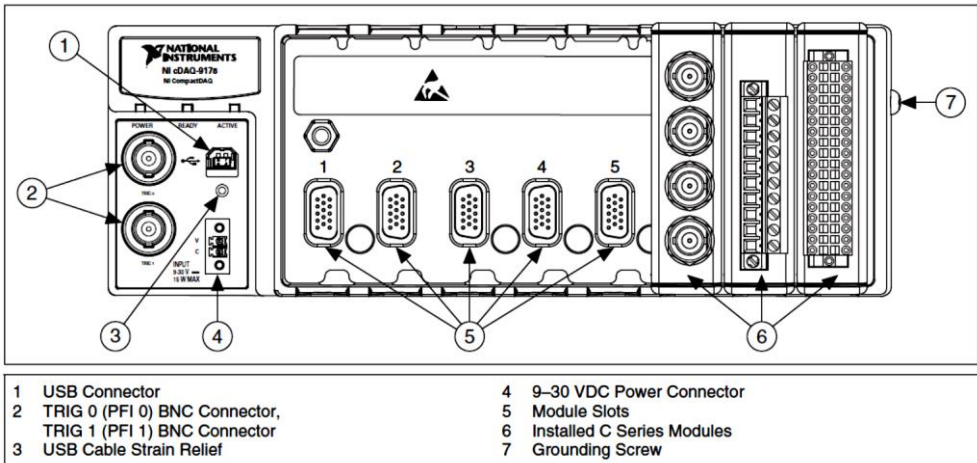


Figure B- 1 NI cDAQ-9178 Chassis

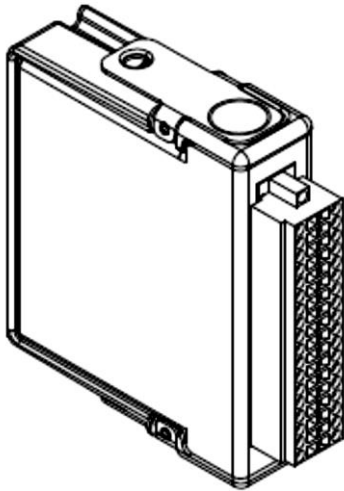


Figure B- 2 NI 9213 16-Channel Thermocouple Input Module

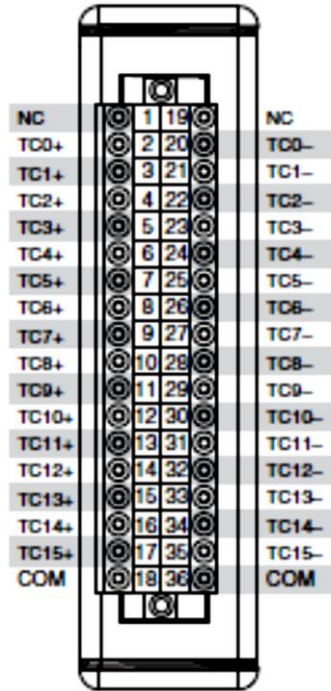


Figure B- 3 NI 9213 Terminal Assignment

The following table includes the technical specifications of the DAQ used.

Component	Specifications		
NI cDAQ-9178	Analog Input	Input FIFO size	127 samples per slot
		Maximum sample rate	6.4 MS/s
		Timing accuracy	50 ppm of sample rate
		Timing resolution	12.5 ns
NI 9213	Input Characteristics	Number of channels	<ol style="list-style-type: none"> 1. 16 thermocouple channels 2. 1 internal auto zero channel, 3. 1 internal cold-junction 4. compensation channel
		ADC resolution	24 bits
		Type of ADC	Delta-Sigma
		Sampling mode	Scanned
		Voltage measurement range	± 78.125 mV
		Temperature measurement ranges	Works over temperature ranges defined by NIST (J, K, T, E, N, B, R, S thermocouple types)
		Timing Mode	<ol style="list-style-type: none"> 1. High-resolution 2. High-speed
		Sample Rate (All Channels)	<ol style="list-style-type: none"> 1. 1 S/s 2. 75 S/s
		Differential input impedance	78 M Ω
		Input current	50 nA
Gain error at High-resolution mode	0.03% typ at 25 °C, 0.07% typ at -40 to 70 °C, 0.15% max at -40 to 70 °C		
Gain error at High-speed mode	0.04% typ at 25 °C, 0.08% typ at -40 to 70 °C, 0.16% max at -40 to 70 °C		

Component	Specifications	
	Offset error	<ol style="list-style-type: none"> 1. High-resolution mode is 4 μV typ, 6 μV max 2. High-speed mode is 14 μV typ, 17 μV max
	Cold-junction compensation accuracy	<ol style="list-style-type: none"> 1. 0 to 70 $^{\circ}\text{C}$0.8 $^{\circ}\text{C}$ typ, 1.7 $^{\circ}\text{C}$ max 2. -40 to 70 $^{\circ}\text{C}$1.1 $^{\circ}\text{C}$ typ, 2.1 $^{\circ}\text{C}$ max
	Measurement sensitivity at High-resolution mode	<ol style="list-style-type: none"> 1. Types J, K, T, E, N...<0.02 $^{\circ}\text{C}$ 2. Types B, R, S<0.15 $^{\circ}\text{C}$
	Measurement sensitivity at the High-speed mode	<ol style="list-style-type: none"> 1. Types J, K, T, E<0.25 $^{\circ}\text{C}$ 2. Type N.....<0.35 $^{\circ}\text{C}$ 3. Type B.....<1.2 $^{\circ}\text{C}$ 4. Types R, S<2.8 $^{\circ}\text{C}$

Furthermore, the data acquisition applications are controlled by software programs. Specialized DAQ software may be delivered with the DAQ hardware. Software tools used for building large-scale data acquisition systems include EPICS, LabVIEW and MATLAB. One of the friendliest software innovated by NI is the LabView Signal Express software which is used in the present study. Signal Express optimizes virtual instrumentation for design engineers by offering instant interactive measurements that require no programming. Signal Express can be used interactively to acquire, generate, analyze, compare, import, and save signals. Moreover, it can compare design data with measurement data in one step. Signal Express extends the ease of use and performance of virtual instrumentation to those who must acquire or analyze signals without programming applications

Appendix C CATALOGUES OF INSTRUMENTATIONS

Appendix A includes the catalogues and manuals of the used equipment and instrumentations.


1. Inline air flow heater

PROCESS AIR & DUCT HEATERS

LOW FLOW AIR PROCESS AND LIQUID CIRCULATION HEATERS

For In-Line Air, Gas and Liquid Heating

AHPF Series

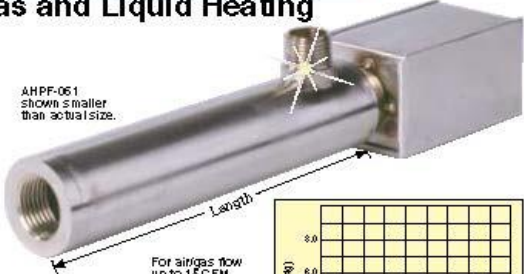


- ✓ 316 Stainless Steel Construction
- ✓ Air/Gas Flow up to 15 CFM
- ✓ Air/Gas Outlet Temperatures up to 430°C (800°F)
- ✓ Pressures up to 100 psi*
- ✓ 50 Watts/Square Inch**

The AHPF Series heaters are used to heat low flows of air, gas, water, or aqueous solutions. Applications include those where clean air is necessary, as in laboratories and environmental testing areas. The stream of air is heated by passing over an enclosed heated surface rather than directly over resistance elements. This method assures that no foreign matter will enter the stream of flow. The AHPF Series is also used as a miniature circulation heater for small volume of liquids as in photographic developer solution, chemicals, dyes, and inks. For heating liquids, contact engineering.

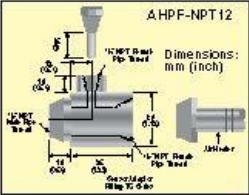
The Thermocouple "T" fitting AHPF-NPT12 can be used with the subminiature thermocouple probes and with the SSLK series stainless steel compression fittings (see omega.com) and with stainless steel compression fittings (Model SSLK-18-14) to monitor or control temperature at the outlet of the AHPF series heaters.

SPECIFICATIONS
 Cross Sectional Area: 0.152 square inches
 Pressure Rating: Up to 100 psig
 Wattage Tolerance: +5, -10% or better at the voltage specified
 Outside Diameter: 32 mm (1 1/4")
 Inlet: Male 1/2" NPT
 Outlet: 3/8" NPT

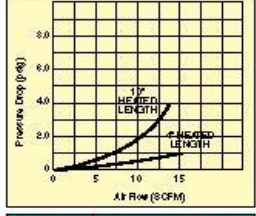


AHPF-051 shows smaller than actual size.

For air/gas flow up to 15 CFM.



AHPF-NPT12 Dimensions: mm (inch)



CFM	Maximum Watts/Inch of Heated Length
1	75
2	100
4	150
6	200
8	200
10	250
15	275

To Order Visit omega.com/ahpf_heater for Pricing and Details

Model Number	Volts	Watts	Heated Length mm (inch)	Watts/ Inch*	Max CFM	Length mm (inch)	Weight kg (lb)
120 Vac Models							
AHPF-061	120	400	102 (4)	91	15	152 (6)	0.45 (1.0)
AHPF-061	120	600	152 (6)	94	15	203 (8)	0.54 (1.18)
AHPF-101	120	1000	203 (8)	120	15	254 (10)	0.62 (1.37)
AHPF-121	120	1200	254 (10)	115	15	305 (12)	0.70 (1.55)
120/240 Volt Models**							
AHPF-062	120	100	102 (4)	23	15	152 (6)	0.45 (1.0)
AHPF-062	240	400	102 (4)	91	15	152 (6)	0.45 (1.0)
AHPF-062	120	150	152 (6)	23	15	203 (8)	0.54 (1.18)
AHPF-062	240	600	152 (6)	94	15	203 (8)	0.54 (1.18)
AHPF-102	120	250	203 (8)	30	15	254 (10)	0.62 (1.37)
AHPF-102	240	1000	203 (8)	120	15	254 (10)	0.62 (1.37)
AHPF-122	120	300	254 (10)	29	15	305 (12)	0.70 (1.55)
AHPF-122	240	1200	254 (10)	115	15	305 (12)	0.70 (1.55)

* Indicates watts per inch of heated length. Use the table above to determine minimum required flow rates. ** These air heaters can be operated on either 120 or 240V. Specifications are shown for either 120 or 240V operation.
 Ordering Example: AHPF-101, 120V, 1000 W low flow air process and liquid circulation heater.

PROCESS AIR & DUCT HEATERS



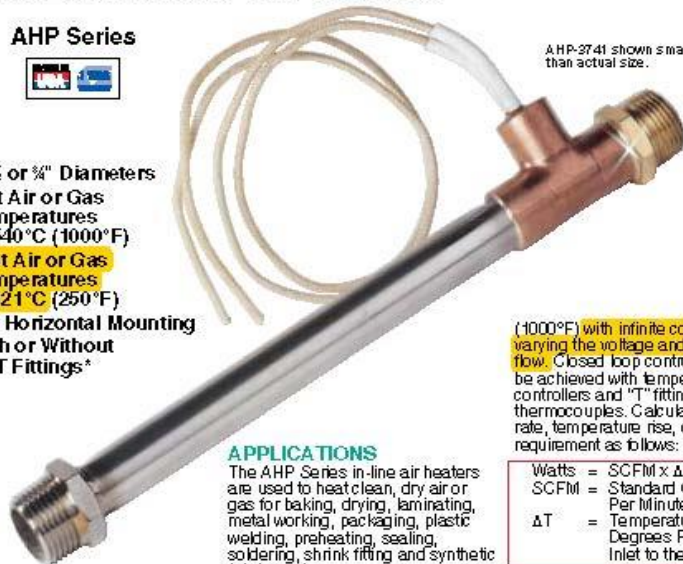
"T" TYPE AIR PROCESS HEATERS

For In-Line Air and Gas Heating

AHP Series



- ✓ ½, ¾ or 1" Diameters
- ✓ Exit Air or Gas Temperatures to 540°C (1000°F)
- ✓ Inlet Air or Gas Temperatures to 121°C (250°F)
- ✓ For Horizontal Mounting
- ✓ With or Without NPT Fittings*



AHP-3741 shown smaller than actual size.

APPLICATIONS

The AHP Series in-line air heaters are used to heat clean, dry air or gas for baking, drying, laminating, metal working, packaging, plastic welding, preheating, sealing, soldering, shrink fitting and synthetic fabric sewing.

AHP series air process heaters provide hot air and gas up to 540°C

(1000°F) with infinite control by varying the voltage and/or the air flow. Closed loop control can also be achieved with temperature controllers and "T" fittings to mount thermocouples. Calculate the flow rate, temperature rise, or power requirement as follows:

$$\begin{aligned} \text{Watts} &= \text{SCFM} \times \Delta T / 3 \\ \text{SCFM} &= \text{Standard Cubic Feet Per Minute} \\ \Delta T &= \text{Temperature Rise in Degrees F from the Inlet to the Outlet} \end{aligned}$$

Maximum flow rates are given in the table below. For minimum flow rates, see table on page 120.

To Order Visit omega.com/ahp_series for Pricing and Details

Model Number	Volts	Watts	Heated Length mm (Inch)	Watts/Inch ²	Maximum CFM	Diameter mm (Inch)	NPT Fitting	Weight g (lb)
120 Vac Models								
AHP-3741	120	200	89 (3½)	57	8	10 (¾)	¼"	82 (0.18)
AHP-5051	120	400	114 (4½)	88	10	13 (½)	¾"	113 (0.25)
AHP-7561	120	750	140 (5½)	136	20	19 (¾)	1"	308 (0.68)
120/240 Vac Models**								
AHP-3742	120 240	80 200	89 (3½) 89 (3½)	14 57	8 8	10 (¾)	¼"	82 (0.18)
AHP-5052	120 240	100 400	11 (4½) 11 (4½)	22 80	10 10	13 (½)	¾"	113 (0.25)
AHP-7562	120 240	190 750	14 (5½) 14 (5½)	34 136	20 20	19 (¾)	1"	308 (0.68)

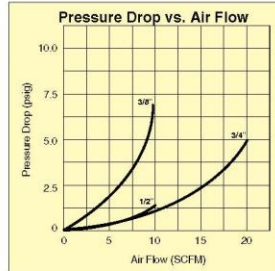
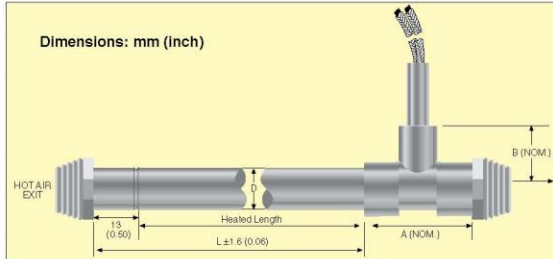
*Note: To order heaters without NPT fittings, add suffix "NF" to model number, price for heaters without fittings is an additional cost for AHP-374 Series, for AHP-505 Series, and for AHP-756 Series.

** These air heaters can be operated on either 120 or 240V. Specifications are shown for operation on both 120 and 240V.

† Indicates watts per inch of heated length. Use the table above to determine minimum required flow rates. The watts per inch of heated length can be changed by reducing the operating voltage or by ordering a custom made heater.

Ordering Example: AHP-3741/120, 200 W, 120 Vac "T" Type in-line air/gas heater.

NEW PROCESS AIR & DUCT HEATERS



Dimensions: mm (inch)

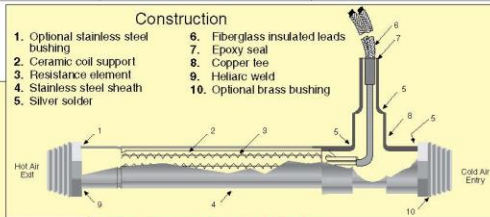
Series	Diameter	Heated Length	L	A	B
AHP-374	9.5 (3/8)	88.9 (3 1/2)	101.6 (4)	7.9 (3/4)	33.3 (1 1/4)
AHP-505	12.7 (1/2)	114.3 (4 1/2)	127.0 (5)	34.9 (1 3/8)	19 (3/4)
AHP-756	19.1 (3/4)	139.7 (5 1/2)	152.4 (6)	61.9 (2 3/8)	41.3 (1 5/8)

SPECIFICATIONS

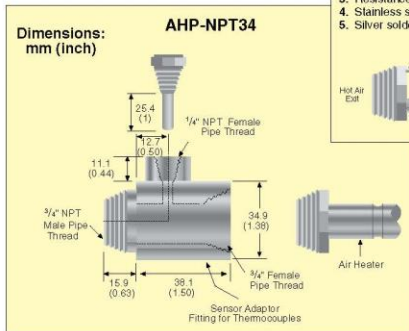
Pressure Rating: 80 psig
 Wattage Tolerance: +5, -10% or better at the voltage specified
 Leads: 0.3 m L (1') fiberglass insulated leads

Maximum Watts Per Linear Inch of Heated Length

Minimum CFM Required	3/8" Diameter	1/2" Diameter	3/4" Diameter
1	60	80	120
2	60	80	120
4	100	100	120
6	150	150	150
8	200	200	200
10	-	250	250
15	-	-	375
20	-	-	500



- Construction**
- Optional stainless steel bushing
 - Ceramic coil support
 - Resistance element
 - Stainless steel sheath
 - Silver solder
 - Fiberglass insulated leads
 - Epoxy seal
 - Copper tee
 - Helic weld
 - Optional brass bushing



Thermocouple T-Fitting

The AHP-NPT34 fitting can be used with subminiature thermocouple probes (see omega.com) and with stainless steel compression fittings (model SSLK-18-14) to monitor temperature at the outlet of the AHP-756 Series heaters.

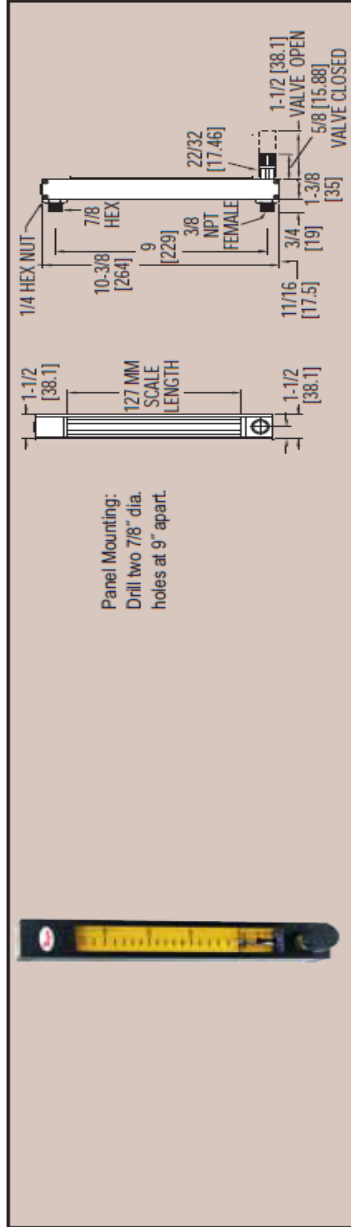
Ordering Example: AHP-NPT34, thermocouple t-fitting.

Model Number

AHP-NPT34

2. Air flow meter

Series DR4
High Flow Glass Flowmeters
 Direct Reading, 127 mm Scale, $\pm 10\%$ FS Accuracy, Interchangeable Floattubes



Series DR4 Glass Flowmeters offer a simplified solution to the problem of fluid flow indication at higher capacity levels. Flowmeters have a direct reading scale for air or water and are designed to withstand even the harshest industrial applications. Permanently fused ceramic scale has integral float guides for optimum float performance. Reflective plastic background and 1.5 X magnification lens reduces eye fatigue and allows for more accurate readings. Units include a safety blow-out back panel for additional protection.

Model (127 mm scale)		With Valve	SS	Flow Rate (Air)	Flow Rate (H ₂ O)
Without Valve	Brass	SS	scfm (SLPM)	GPM (LPM)	
DR4101	DR4141	DR4241	0.2-4 (5-120)	-	-
DR4103	DR4143	DR4243	0.5-11 (20-320)	-	-
DR4104	DR4144	DR4244	1-16 (20-500)	-	-
DR4106	DR4146	DR4246	-	0.1-2 (0.5-8)	-
DR4108	DR4148	DR4248	-	0.2-4 (1-16)	-
DR4109	DR4149	DR4249	-	0.5-5 (1-22)	-

Air Flow meters
DR4104

SPECIFICATIONS
Service: Compatible gases or liquids.
Wetted Materials: Flowtube: Borosilicate glass; Float: 316 SS; Float stops: PTFE; Floats: Brass or 316 SS; Connections: Buna-N on brass models and fluor elastomer on SS models.
Temperature Limits: 250°F (121°C).

Pressure Limits: 200 psig (13.8 bar).
Accuracy: $\pm 10\%$ FS @ 70°F (21.1°C) and 14.7 psia (1 atm absolute).
Repeatability: $\pm 0.25\%$ of scale reading.
Scale: Direct reading 127 mm scales for air or water.
Turn-down Ratio: 10:1.
Connection: 3/8" female NPT.
Mounting: Vertical.
Valve: 6-turn needle (standard on models with valve).

Add suffix "M" for metric scale.



3. Fuel injector

DELAVAN PRECISION OIL BURNER NOZZLES

DELAVAN
ProTek™
 NOZZLE SYSTEM

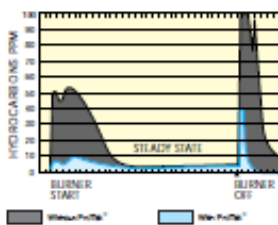
SMART VALVE
 DESIGN REDUCES
 COMBUSTION
 POLLUTION FOR
 CLEANER HEATING



The all-new Delavan ProTek™ Nozzle System provides the first step into the future of Clean Air Technology™. This unique, patented System from Delavan provides significant reductions in combustion pollutants for cleaner air. The ProTek Nozzle System includes a factory-installed, one-piece Valve Component which reduces smoke and oil smell in the off cycle by preventing oil after-drip from the nozzle. Also, the reduction of smoke (carbon and soot) helps maintain burner set up efficiency longer and extend the time period between appliance clean ups.

Installation is fast and easy; there's no need to increase pump supply pressure at installation because there's no pressure drop. Plus, ProTek Nozzle Systems maintain the same flow pattern and flow rating characteristics of comparably rated Delavan nozzles.

The dramatic benefits of the ProTek Nozzle System are available in either a factory-installed, complete system or as the ProTek Valve Component sold separately to replace the standard filter on a Delavan nozzle.



Hydrocarbon emissions are greatly reduced when the Delavan ProTek™ Nozzle System is used. Hydrocarbons are typically elevated at start-up and shut-down of the nozzle firing, as both of these graphs show. When the ProTek Nozzle System is installed, the dramatic benefits are seen in these charts which show comparative results with and without the ProTek™ valve. Results will vary by application.

TEK TALK

The Delavan ProTek™ Nozzle System has been thoroughly tested. In the tests, approximately seven years of "on/off" cycle operation simulation in the laboratory with no failures. A total of 107,000 cycles were recorded. After the first 11,350 cycles, the cut-on pressures shifted upward an average of 3.0 PSI. The cut off pressure shifted up an average of 7.75 PSI. After this initial seating process, there was very little change of either "on" or "off" pressures. Very little change in nozzle flow was noted after 107,000 cycles, either. Additional testing has included pressure tests up to 500 PSI (34.5 BAR), as well as combustion tests and tests with various fuels such as kerosene, #2, and heavier oils. Detailed test results are available from Delavan Technical Services.

Operating Pressures

Valve Part #	Minimum Operating Pressures		
	Supply Pump PSI (BAR)	Valve Open PSI (BAR)	Valve Close PSI (BAR)
60030-1	135.0 (9.3)	125.0 (8.6)	65.0 (4.5)
60030-2	100.0 (7.0)	60.0 (4.1)	45.0 (3.1)

عند مخرج غرفة الاحتراق للحارقين. وقد تمت مقارنة خواص اللهب الناتج من تلك المخاليط مع خواص اللهب الناتج من حرق وقود الطائرات منفردا وأظهرت النتائج أن توزيع درجة حرارة اللهب الموضعية لمخاليط الوقود الحيوي مع وقود الطائرات لا تختلف كثيرا عن توزيع درجة الحرارة اللهب الناتج من الوقود الطائرات. ويمكن استنتاج أن إضافة الوقود الحيوي إلى وقود الطائرات له تأثير كبير على خصائص الانبعاثات لاحتراق مسبق التبخر والخلط حيث انخفضت انبعاثات أول أكسيد الكربون وأكاسيد النتروجين عند مخرج غرفة الاحتراق بشكل ملحوظ بنسبة 70% و58% على الترتيب، مقارنة بقيم انبعاثات حرق وقود الطائرات. لذلك يمكن استبدال وقود الطائرات بمزيج الوقود الحيوي مع وقود الطائرات دون عمل أي تعديلات في تصميم غرفة الاحتراق نظرا لأن له نفس توزيع درجات الحرارة وتحسين كبير للانبعاثات.

الملخص

أن الحد من الانبعاثات الناتجة من أنظمة الحريق المختلفة والبحث عن مصادر بديلة للطاقة تعد من أهم التحديات العلمية على مستوى العالم أجمع. وفي نفس الوقت فإن استخدام الوقود الحيوي الناتج من زيوت الطعام المهذرة يعد أحد أفضل الحلول لهذه التحديات. تستخدم عملية هدرجة الزيوت النباتية في إنتاج الوقود البديل من الزيت الخام وذلك بواسطة جهاز الخلط بالموجات فوق الصوتية لتقليل زمن عملية الإنتاج.

في ذلك السياق فإن هذه الدراسة تنقسم إلى مجموعتين مختلفتين من التجارب. في المجموعة الأولى من التجارب تقارن الدراسة ظروف التدفق البارد (الهواء)، هيكل اللهب، الاحتراق، والانبعاثات الناتجة من حرق وقود الطائرات عن طريق استخدام حارقين دوامات لهم رقم تدويم متطابق (SN = 0.55) وتصميمين مختلفين. التصميم الأول حارق عالي التدويم في حين أن الثاني هو حارق منخفض التدويم مع لوحة مركزية مثقبة تسمح بتدفق محوري من خلال مركز الموقد. تحدد المجموعة الثانية من التجارب تأثير حرق خليط من وقود الديزل الحيوي مع وقود الطائرات في غرفة احتراق توربينة غازية على خصائص اللهب وانبعاثات العادم. يتم خلط وقود الديزل الحيوي مع وقود الطائرات بنسب حجمية 5، 10، 15 و 20٪ ويرمز لها بـ B5، B10، B15 و B20 على التوالي. لجميع الحالات التي تم اختبارها تستخدم تقنية الاحتراق المضطرب مسبق الخلط والتبخير مع الحفاظ على درجة حرارة خليط الوقود / الهواء الداخل إلى غرفة الاحتراق عند درجة حرارة 250 درجة مئوية مع نسبة تكافؤ $\phi = 0.75$.

وتشير النتائج الرئيسية إلى أن مجال السريان للحارق منخفض الدوامات خال من منطقة إعادة التدوير المركزية في حين أن الحارق عالي التدويم يكون منطقة إعادة تدوير مركزية كبيرة. الحارقين لهم كفاءة احتراق متماثلة ويمكن للحارق عالي التدويم توليد لهب أزرق على شكل مخروط في حين أن الحارق منخفض الدوامات يولد لهب أزرق على شكل حرف "W". يظهر توزيع درجة حرارة لهب الحارق عالي الدوامات منطقة درجة حرارة عالية علي حافة الموقد والتي تمثل بقعة ساخنة في حين أن اللهب الناتج من الحارق منخفض الدوامات يظهر توزيع درجة حرارة أكثر تماثل. نسبة انبعاثات أول أكسيد الكربون وأكاسيد النتروجين للحارق منخفض التدويم خلال اللهب أقل بنسبة 50% بالمقارنة باللهب الناتج من الحارق عالي التدويم في حين أنها متقاربة

قامت اللجنة بتحكيم الرسالة تحت عنوان

دراسة الذهب المستقر للوقود الحيوي سابق الخلط والتبخير

المقدمة من المهندس

بلال يحيى ابراهيم السعيد بلال

بكالوريوس الهندسة والتكنولوجيا في الهندسة الميكانيكية، شعبة طاقة، 2014

كجزء من متطلبات الحصول على درجة الماجستير

في العلوم الهندسية في الهندسة الميكانيكية

أُعتمدت وأجيزت من لجنة الحكم والمناقشة

(رئيساً)

أ.د./ محمود عبد الرشيد نصير

أستاذ متفرغ بقسم الهندسة الميكانيكية

كلية الهندسة - جامعة عين شمس

(عضواً)

أ.د./ سعد الدين محمد السعيد حابك

أستاذ متفرغ بقسم الهندسة الميكانيكية

كلية الهندسة - جامعة بورسعيد

(عضواً)

أ.د./ هاني أحمد منيب

أستاذ متفرغ بقسم هندسة القوى الميكانيكية

كلية الهندسة بالمطرية-جامعة حلوان

(عضواً)

أ.د./ هشام محمد على البطش

الأستاذ بقسم الهندسة الميكانيكية

كلية الهندسة ببنها-جامعة بنها

(رئيس القسم)

اعتمدت من قسم الهندسة الميكانيكية

أ.م.د./ أحمد عبد الفتاح البيطار

(وكيل الكلية للدراسات العليا)

اعتمدت من الدراسات العليا

أ.د./ هشام محمد على البطش

(عميد الكلية)

اعتمدت من الكلية

أ.د./ عارف محمد أحمد سليمان



جامعة بنها كلية الهندسة بنها



قسم الهندسة الميكانيكية

دراسة الذهب المستقر للوقود الحيوي سابق الخلط والتبخير

رسالة مقدمة للحصول على درجة الماجستير في العلوم الهندسية في الهندسة
الميكانيكية

إعداد

بلال يحيى ابراهيم السعيد بلال

بكالوريوس الهندسة والتكنولوجيا في الهندسة الميكانيكية، شعبة الطاقة، 2014

المشرفون

أ.د/ هشام محمد البطش
أستاذ نظم الطاقة بقسم الهندسة الميكانيكية
كلية هندسة بنها
جامعة بنها

أ.د/ هاني أحمد منيب
أستاذ متفرغ بقسم هندسة القوى الميكانيكية
كلية الهندسة بالمطرية
جامعة حلوان

أ.م.د/ على محمود عطية
أستاذ مساعد بقسم الهندسة الميكانيكية
كلية هندسة بنها
جامعة بنها

بنها 2018